ENCLOSURE B

DB-1 CRDM NOZZLE J-GROOVE WELD FLAW EVALUATION FOR IDTB REPAIR

(NONPROPRIETARY VERSION)

AREVA CALCULATION 32-9136508-002

Fifty-Nine Pages Follow

AREVA

CALCULATION SUMMARY SHEET (CSS)

Document No. 32 - 9136508 - 002 Safety Related: ☒ Yes ☐ No

Title DB-1 CRDM Nozzle J-Groove Weld Flaw Evaluation for IDTB Repair

PURPOSE AND SUMMARY OF RESULTS:

Purpose

This document is a non-proprietary version of AREVA NP Document 32-9134664-003. The AREVA NP proprietary information removed from 32-9134664-003 is indicated by a pair of braces "{ }".

The purpose of the present analysis is to determine from a fracture mechanics viewpoint the suitability of leaving degraded J-groove weld and butter material in the Davis Besse Unit 1 reactor vessel head following the repair of a Control Rod Drive Mechanism (CRDM) nozzle by the ID temper bead weld procedure. It is postulated that a small flaw in the head would combine with a large stress corrosion crack in the weld and butter to form a radial corner flaw that would propagate into the low alloy steel head by fatigue crack growth under cyclic loading conditions.

The purpose of Revision 2 is to change the full load core exit temperature to { } °F.

Summary of Results

Based on a combination of linear elastic and elastic plastic fracture mechanics analysis of a postulated remaining flaw in the original Alloy 182 J-groove weld and butter material, a Davis Besse Unit 1 CRDM nozzle is considered to be acceptable for at least 4 years of operation following an IDTB weld repair. The controlling loading condition was determined to be the rod withdrawal transient, for which it was shown that with safety factors of 3 on primary loads and 1.5 on secondary loads that the applied tearing modulus (11.63) was still less than the tearing modulus of the low alloy steel head material (12.88).

*This document consists of pages 1 – 46, A-1, B-1 – B-3, C-1 – C-4, D-1 – D-3, and E-1 – E-2.

[redacted]

THE FOLLOWING COMPUTER CODES HAVE BEEN USED IN THIS DOCUMENT:		THE DOCUMENT CONTAINS ASSUMPTIONS THAT SHALL BE VERIFIED PRIOR TO USE
CODE/VERSION/REV	CODE/VERSION/REV	☐ YES
ANSYS/10/0		☒ NO

AREVA
AREVA NP Inc.,
an AREVA and Siemens company

0402-01-F01 (20697) (Rev. 014, 04/13/2009)

Document No. 32-9136508-002

DB-1 CRDM Nozzle J-Groove Weld Flaw Evaluation for IDTB Repair

Review Method: ☒ Design Review (Detailed Check)
☐ Alternate Calculation

Signature Block

Name and Title (printed or typed)	Signature	P/R/A and LP/LR	Date	Pages/Sections Prepared/Reviewed/Approved
D. E. Killian Technical Consultant	D. E. Killian	P	5/10/10	All
S. J. Noronha Engineer IV	S J Noronha	R	5/10/10	All
T. M. Wiger Unit Manager	T. M. Wiger	A	5/11/10	All

Note: P/R/A designates Preparer (P), Reviewer (R), Approver (A);
LP/LR designates Lead Preparer (LP), Lead Reviewer (LR)

Project Manager Approval of Customer References (N/A if not applicable)

Name (printed or typed)	Title (printed or typed)	Signature	Date
R. J. Baker, Jr.	Project Manager	RJ Baker	5/4/10

Mentoring Information (not required per 0402-01)

Name (printed or typed)	Title (printed or typed)	Mentor to: (P/R)	Signature	Date
N/R				

Record of Revision

Revision No.	Date	Pages/Sections/ Paragraphs Changed	Brief Description / Change Authorization
000	04/2010	All	Original release
001	04/2010	Throughout	Changed indicator for proprietary information from square brackets ("[ ]") to braces ("{ }")
002	05/2010	Pages 25-26, 30, 32-46, B-1 – B-3, D-2, D-3, E-1	Calculations modified to reflect a full load core exit temperature of { } °F

Table of Contents

Table of Contents
(continued)

List of Tables

List of Figures

1.0 INTRODUCTION

A March 2010 inspection of Alloy 600 control rod drive mechanism (CRDM) nozzles in the reactor vessel closure head (RVCH) at Davis Besse Unit 1 revealed defects in several nozzles and nozzle-to-RVCH partial penetration welds, along with evidence of leakage as manifested by deposits of boric acid crystals on the outer surface of the head. The original RVCH at Davis Besse Unit 1 (DB-1) was replaced in 2002 with the closure head from a suspended Midland plant owned by Consumers Power Company. It is currently believed that the leakage in the DB-1 RVCH was caused by primary water stress corrosion cracking (PWSCC) of the susceptible Alloy 600 nozzles and Alloy 182 welds. Degraded nozzles at DB-1 are to be repaired using an inside diameter temper bead (IDTB) welding procedure wherein the lower portion of a nozzle is removed by a boring procedure and the remaining portion of the nozzle is welded to the low alloy steel reactor vessel head above the original Alloy 182 J-groove attachment weld, as shown in Figure 1-1. The repair is more fully described by the design drawing [1] and the design specification [2]. Although the remnant J-groove weld would no longer be associated with the primary pressure boundary, a defect in the weld could grow into the low allow steel RVCH and thereby impact the structural integrity of the remaining pressure boundary. Since a potential, or even detected, flaw in the J-groove weld can not be sized by currently available non-destructive examination techniques, it is assumed that the "as-left" condition of the remnant J-groove weld includes degraded or cracked weld material extending through the entire J-groove weld and Alloy 182 butter material.

Since it is known from analysis of the original Davis Besse Unit 1 CRDM reactor vessel head nozzle penetrations [3] that the hoop stress in the J-groove weld is greater than the axial stress at the same location, the preferential direction for cracking would be axial, or radial relative to the nozzle. Reference 3 also demonstrates that stresses tend to be higher on the uphill side of the nozzles than on the downhill side. It is postulated that a radial crack in the Alloy 182 weld metal would propagate by PWSCC, through the weld and butter, to the interface with the head material, where it is fully expected that such a crack would then blunt, or arrest, as discussed in Reference 4 for interfaces with low alloy steels. Since the height of the weld and butter along the bored surface is about 2" on the uphill side of the outermost CRDM nozzle, a radial crack depth extending from the corner of the weld to the low alloy steel head would be very deep. Although primary water stress corrosion cracking would not extend into the head, it is further postulated that a small fatigue initiated flaw forms in the low alloy steel head and combines with the stress corrosion crack in the weld to form a large radial flaw that would propagate into the head by fatigue crack growth under cyclic loading conditions. Linear-elastic (LEFM) and elastic-plastic (EPFM) fracture mechanics procedures are utilized to evaluate this worst case flaw in the original J-groove weld and butter.

Key features of the fracture mechanics analysis are:

- This analysis applies specifically to the CRDM nozzle penetrations in the Davis Besse Unit 1 reactor vessel closure head. A J-integral resistance curve is developed based on estimates of the Charpy V-notch upper-shelf energy for the DB-1 head plate material.
- Flaw growth is calculated for a 4 year period of operation, corresponding to 2 fuel cycles.
- Flaw acceptance is based on the available fracture toughness and ductile tearing resistance of the RVCH material considering the safety factors listed in Table 1-1.

Table 1-1: Safety Factors for Flaw Acceptance

Linear-Elastic Fracture Mechanics			
Operating Condition	Evaluation Method	Fracture Toughness / K_I	
Normal/Upset	K_{Ia} fracture toughness	$\sqrt{10} = 3.16$	
Emergency/Faulted	K_{Ic} fracture toughness	$\sqrt{2} = 1.41$	
Elastic-Plastic Fracture Mechanics			
Operating Condition	Evaluation Method	Primary	Secondary
Normal/Upset	J/T based flaw stability	3.0	1.5
Normal/Upset	$J_{0.1}$ limited flaw extension	1.5	1.0
Emergency/Faulted	J/T based flaw stability	1.5	1.0
Emergency/Faulted	$J_{0.1}$ limited flaw extension	1.5	1.0

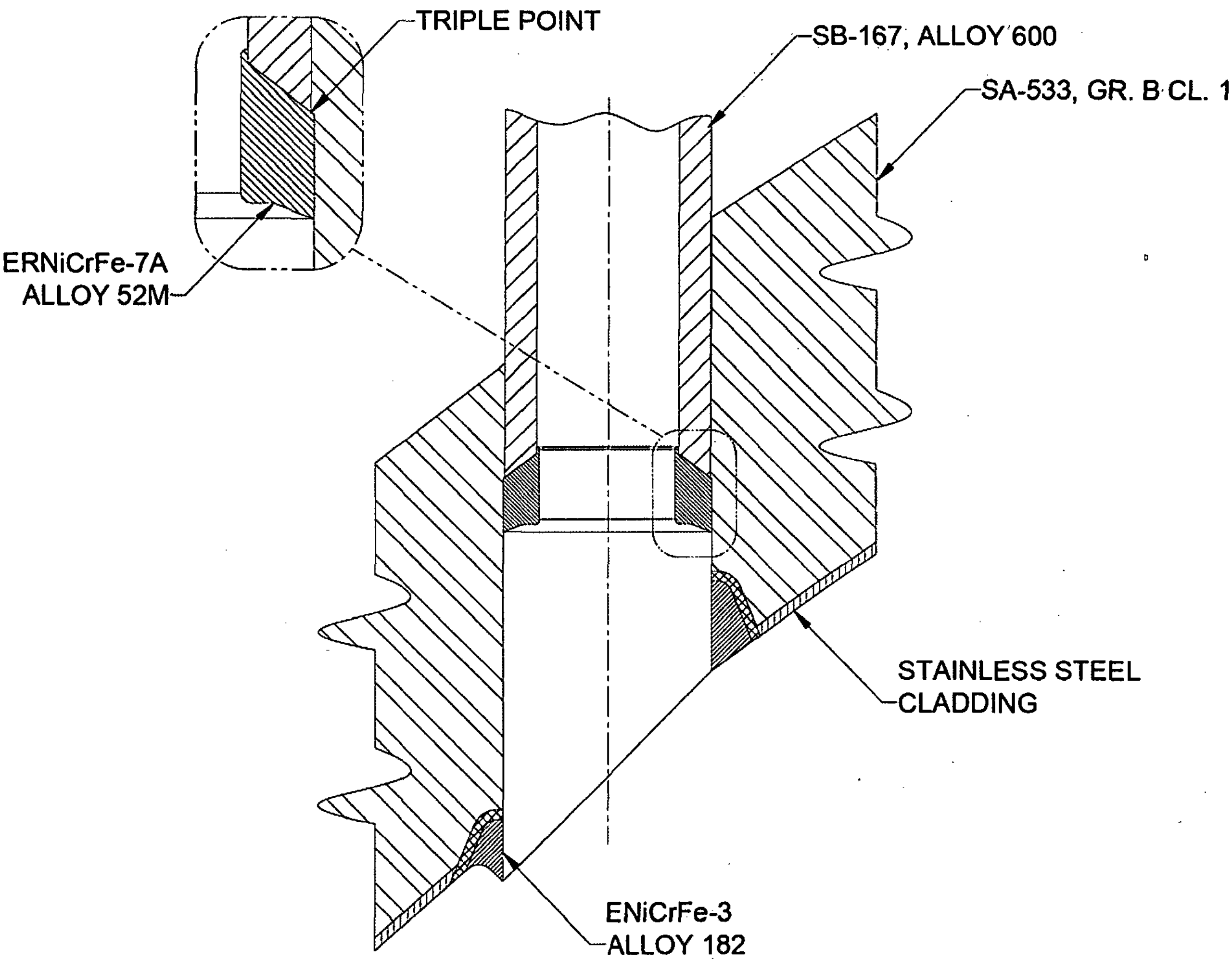

Figure 1-1: ID Temper Bead Weld Repair

2.0 ANALYTICAL METHODOLOGY

A radial flaw at the inside corner of non-radial head penetration is evaluated based on a combination of linear-elastic fracture mechanics (LEFM) and elastic-plastic fracture mechanics (EPFM), as outlined below.

1. Postulate a radial flaw in the J-groove weld, extending from the inside corner of the penetration to the interface between the butter and head, as shown in Figure 2-1 for the uphill side of the penetration. Previous analysis [5] has shown that even for large downhill welds, the controlling location is the uphill side of the penetration, due to higher stresses and the additional constraint provided by the acute angle between the material borders along the cladding and bore.

2. Develop a three-dimensional finite element crack model of the reactor vessel head in the vicinity of the outermost nozzle penetration, with crack tip elements along the interface between the Alloy 182 butter and the low alloy steel base metal. This crack model will be used to obtain stress intensity factors at various positions along the crack front for combined stresses due to J-groove welding, hydrostatic testing, nozzle removal, and transient loading conditions.

3. Develop a mapping procedure to transfer stresses from uncracked finite element stress analysis models (for residual and operational stresses) to the crack face of the crack model. This will enable stress intensity factors to be calculated for arbitrary stress distributions over the crack face utilizing the principle of superposition.

4. Calculate fatigue crack growth for cyclic loading conditions using combined residual and operational stresses from pressure and thermal loads. It is noted that the only effect of residual stress on fatigue crack growth is in the calculation of the R ratio, or K_{min}/K_{max}, which is the ratio of the minimum and maximum stress intensity factors for a pair of stress states. Starting from the stress intensity factor calculated by the finite element crack model for the initial flaw size, stress intensity factors are updated for each increment of crack growth by the square root of the ratio of the flaw sizes over the increment.

5. Utilize the screening criteria of ASME Code Section XI, Appendix H to determine the failure mode and appropriate method of analysis (LEFM or EPFM) for flaws in ferritic materials, considering the applied stress, temperature, and material toughness. For LEFM flaw evaluations, compare the stress intensity factor at the final flaw size to the available fracture toughness, with appropriate safety factors, as discussed in Section 2.2. When the material is more ductile and EPFM is the appropriate analysis method, evaluate flaw stability and crack driving force as described in Section 2.3.

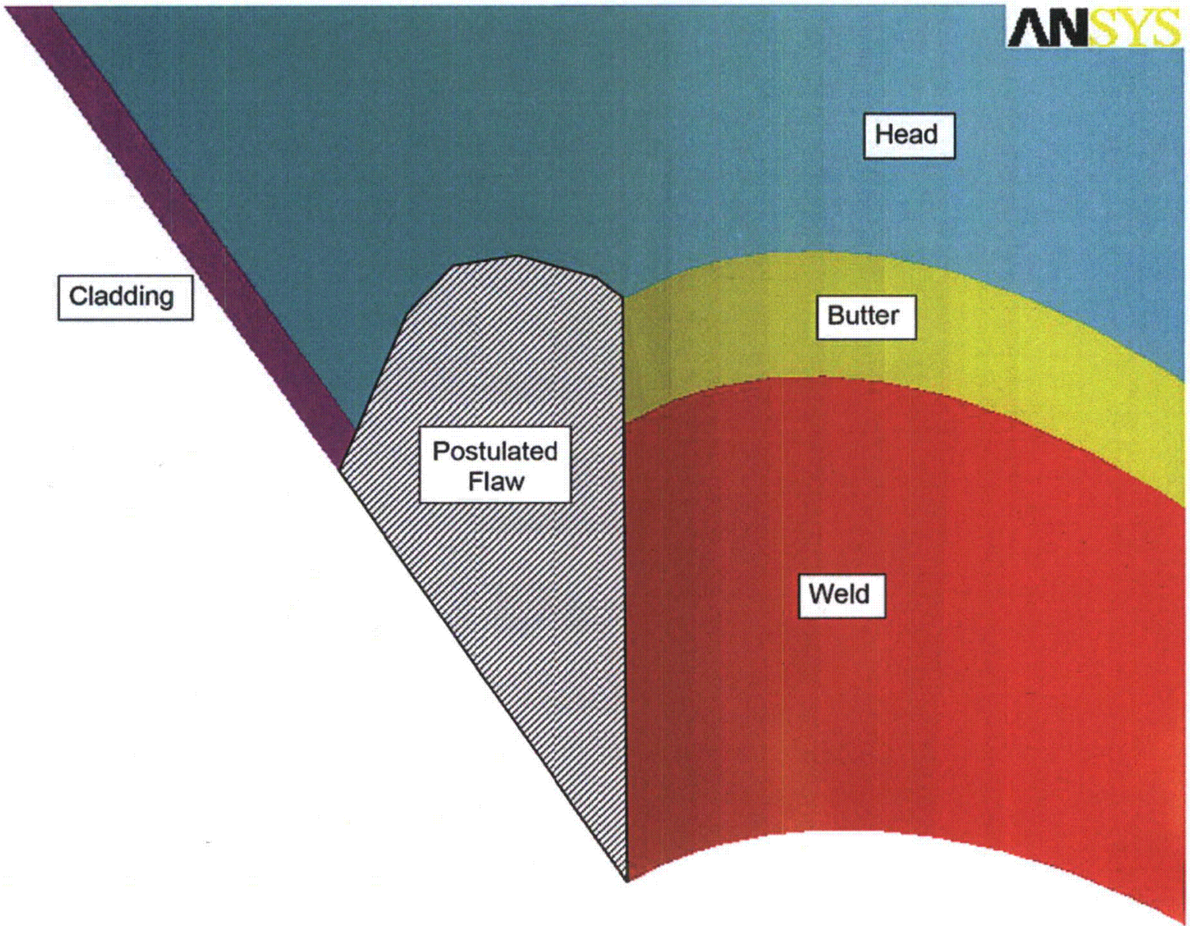

Figure 2-1: Postulated Radial Flaw on Uphill Side

2.1 Stress Intensity Factor Solution

Stress intensity factors for corner flaws at a non-radial nozzle penetration are best determined by finite element analysis using three-dimensional models with crack tip elements along the crack front. Although loads can be applied to finite element crack models like any other structural model, the crack model was developed to serve as a flaw evaluation tool that could accept stresses from separate stress analyses. This strategy makes it possible, for example, to obtain pressure and thermal stresses from an independent thermal/structural analysis and then transfer these stresses to a crack model for flaw evaluations. Using the principle of superposition common to fracture mechanics analysis, the only stresses that need be considered for these flaw evaluations are the stresses on the crack face. A mapping procedure is developed to transfer stresses from a separate stress analysis to the crack face of the crack model.

2.1.1 Finite Element Crack Model

A three-dimensional finite element model is developed for the reactor vessel head in the vicinity of the outermost nozzle penetration, by modeling a portion of the head, cladding, and butter with the ANSYS finite element computer program [6]. Since stresses increase with penetration angle, it is conservative to base the model on the outermost nozzle penetration. Details of the finite element crack models are presented in Appendix A.

The three-dimensional finite element model is first constructed to represent an unflawed non-radial nozzle penetration in the reactor vessel head using the ANSYS SOLID95 20-node structural element. Elements along the crack front are then replaced by a sub-model of crack tip elements along the interface between the Alloy 182 butter and the low alloy steel base metal. These elements consist of 20-node isoparametric elements that are collapsed to form a wedge with the appropriate mid-side nodes shifted to quarter-point locations to simulate a singularity at the crack tip. The final crack model is shown in Figure 2-2.

Stress intensity factors are obtained using the ANSYS KCALC routine at 10 positions along each crack front, as indicated in Figure 2-2. Position 1 in located on the cladding surface, Position 2 at the cladding/base metal interface, and Position 10 is at the bored surface in the head.

2.1.2 Stress Mapping

Residual and operational stresses, obtained from separate finite element models, are mapped onto the crack face of the finite element crack model shown in Figure 2-2 to calculate the individual contributions to the stress intensity factors. A set of ANSYS parametric design language instructions (macro) has been written based on the *MOPER,MAP command to transfer stresses by nodal interpolation from a dissimilar finite element model (e.g., residual stresses) to the crack model. Stresses from an identical finite element model (e.g., operational stresses), are simply copied from the stress model to the crack model.

Key Position Indicators for Stress Intensity Factors

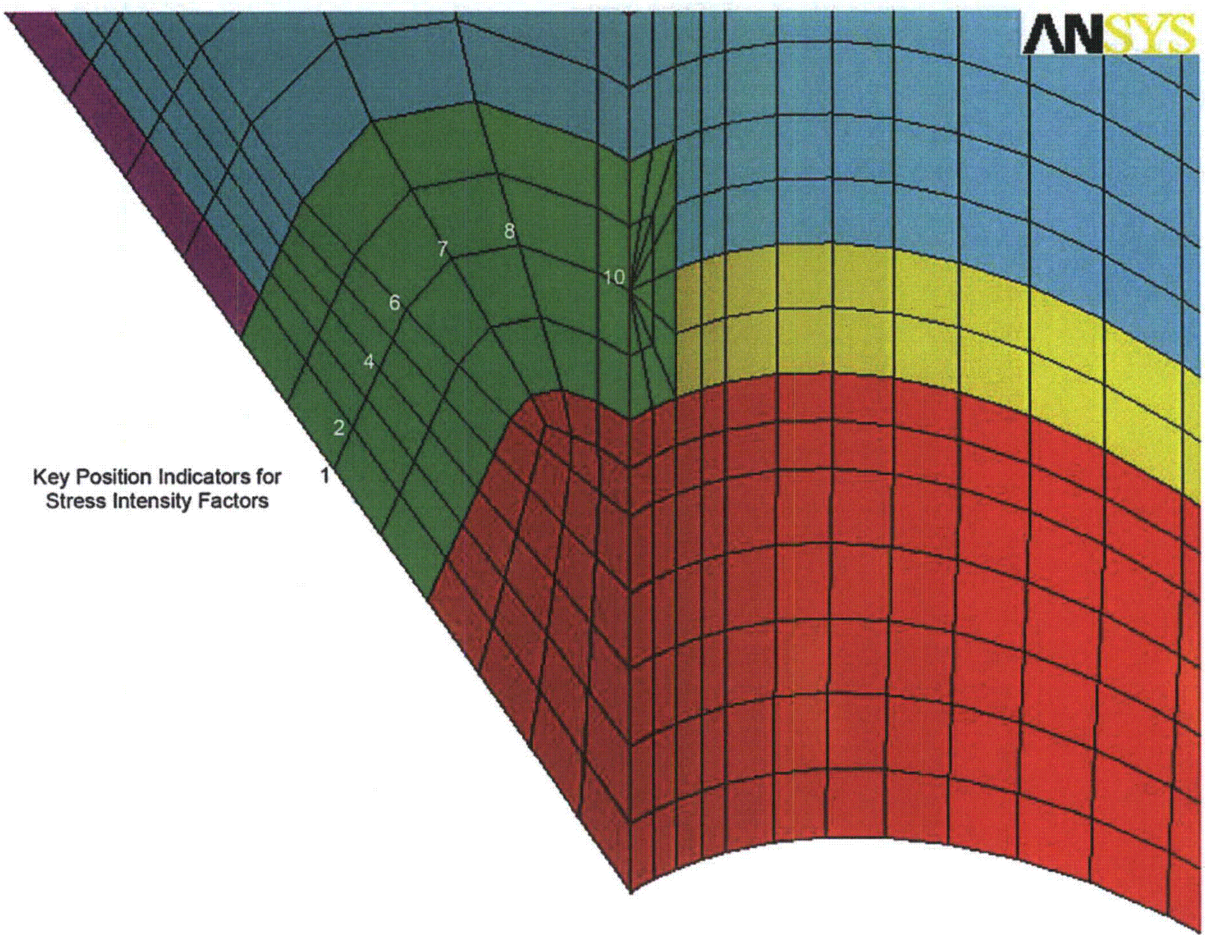

Figure 2-2: Finite Element Crack Model

2.1.3 Crack Growth Considerations

The fundamental expression for the crack tip stress intensity factor is

$$K_I = \sigma\sqrt{\pi a}$$

Since the crack model is developed for a single flaw size, stress intensity factors are updated at each increment of crack growth by the square root of the flaw size; i.e.,

$$K_I(a_{i+1}) = K_I(a)\sqrt{\frac{a_{i+1}}{a_i}},$$

where

a = flaw size

i = increment of crack growth.

Since the stress intensity factor is directly proportional to the magnitude of the stress and both residual and operating stresses decrease in the direction of crack growth, this procedure produces conservative estimates of stress intensity factor as the crack extends into the head and stresses diminish over the expanding crack face.

2.1.4 Plastic Zone Correction

The Irwin plasticity correction is used to account for a moderate amount of yielding at the crack tip. For plane strain conditions, this correction is

$$r_y = \frac{1}{6\pi}\left(\frac{K_I(a)}{\sigma_y}\right)^2, \qquad \text{[Ref. [7] , Eqn. (2.63)]}$$

where $K_I(a)$ = stress intensity factor based on the actual crack size, a

σ_y = material yield strength.

A stress intensity factor, $K_I(a_e)$, is then calculated for an effective crack size,

$$a_e = a + r_y,$$

based on the same scaling technique utilized for crack growth; i.e.,

$$K_I(a_e) = K_I(a)\sqrt{\frac{a_e}{a}}.$$

2.2 Linear-Elastic Facture Mechanics

Article IWB-3612 of Section XI [11] requires that the applied stress intensity factor, K_I, at the final flaw size be less than the available fracture toughness at the crack tip temperature, with appropriate safety factors, as outlined below.

Normal and upset conditions: $K_I < K_{Ia} / \sqrt{10}$

where K_{Ia} is the fracture toughness based on crack arrest.

Emergency and faulted conditions: $K_I < K_{Ic} / \sqrt{2}$

where K_{Ic} is the fracture toughness based on crack initiation.

2.3 Elastic-Plastic Facture Mechanics

Elastic-plastic fracture mechanics (EPFM) will be used as alternative acceptance criteria when the flaw related failure mechanism is unstable ductile tearing. This type of failure falls between rapid, non-ductile crack extension and plastic collapse. Linear-elastic fracture mechanics (LEFM) would be used to assess the potential for non-ductile failure, whereas limit load analysis would be used to check for plastic collapse.

2.3.1 Screening Criteria

Screening criteria for determining failure modes in ferritic materials may be found in Appendix H of Section XI. Although Appendix H, Article H-4200 [11] contains specific rules for evaluating flaws in Class 1 ferritic piping, its screening criteria may be adapted to other ferritic components, such as the reactor vessel head, as follows:

Let, $K_r' = K_{Iapp} / K_{Ic}$

$S_r' = \sigma_{max} / \sigma_f$

Then the appropriate method of analysis is determined by the following limits:

LEFM Regime:	$K_r' / S_r' \geq 1.8$
EPFM Regime:	$1.8 > K_r' / S_r' \geq 0.2$
Limit Load Regime:	$0.2 > K_r' / S_r'$

2.3.2 Flaw Stability and Crack Driving Force

Elastic-plastic fracture mechanics analysis will be performed using a J-integral/tearing modulus (J-T) diagram to evaluate flaw stability under ductile tearing, where J is either the applied (J_{app}) or the material (J_{mat}) J-integral, and T is the tearing modulus, defined as $(E/\sigma_f^2)(dJ/da)$. The crack driving force, as measured by J_{app}, is also checked against the J-R curve at a crack extension of 0.1 inch ($J_{0.1}$). Consistent with industry practice for the evaluation of flaws in partial penetration welded nozzles, different safety factors will be utilized for primary and secondary loads. Flaw stability assessments for normal and upset conditions will consider a safety factor of 3 on the stress intensity factor due to primary (pressure) stresses and a safety factor of 1.5 for secondary (residual plus thermal) stresses. The crack driving force will be calculated using safety factors of 1.5 and 1 for primary and secondary stresses, respectively. For EPFM analysis of faulted conditions, safety factors of 1.5 and 1 will be used for flaw stability assessments and 1.5 and 1 for evaluations of crack driving force.

The general methodology for performing an EPFM analysis is outlined below.

Let $E' = E/(1-\nu^2)$

Final flaw depth $= a$

Total applied K_I $= K_{Iapp}$

K_I due to pressure (primary) $= K_{Ip}$ (from Appendix B)

K_I due to residual plus thermal (secondary) $= K_{Is} = K_{Iapp} - K_{Ip}$

Safety factor on primary loads $= SF_p$

Safety factor on secondary loads $= SF_s$

For small scale yielding at the crack tip, a plastic zone correction is used to calculate an effective flaw depth based on

$$a_e = a + [1/(6\pi)]\,[\,(K_{Ip} + K_{Is}) / \sigma_y\,]^2,$$

which is used to update the stress intensity factors based on

$$K'_{Ip} = K_{Ip}\sqrt{\frac{a_e}{a}}$$

and

$$K'_{Is} = K_{Is}\sqrt{\frac{a_e}{a}}.$$

The applied J-integral is then calculated using the relationship

$$J_{app} = (SF_p{*}K'_{Ip} + SF_s{*}K'_{Is})^2/E'.$$

The final parameter needed to construct the J-T diagram is the tearing modulus. The applied tearing modulus, T_{app}, is calculated by numerical differentiation for small increments of crack size (da) about the final crack size (a), according to

$$T_{app} = \frac{E}{\sigma_f^2}\left[\frac{J_{app}(a+da) - J_{app}(a-da)}{2(da)}\right].$$

Using the power law expression for the J-R curve,

$$J_{mat} = C(\Delta a)^m,$$

the material tearing modulus, T_{mat}, can be expressed as

$$T_{mat} = (E/\sigma_f^2)Cm(\Delta a)^{m-1}.$$

Constructing the J-T diagram,

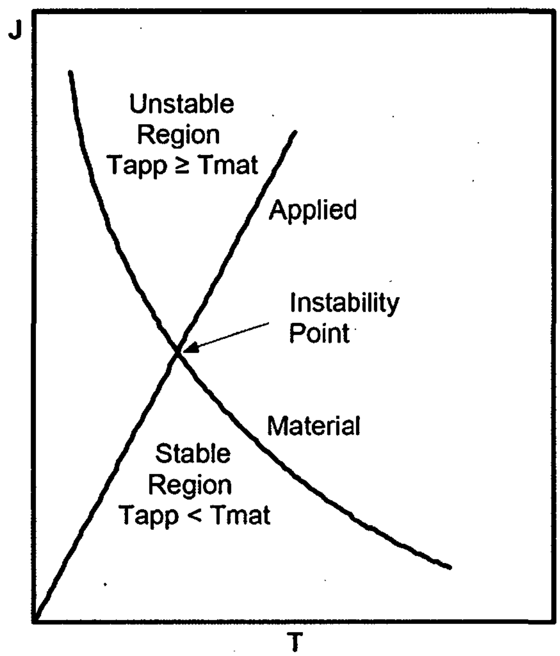

flaw stability is demonstrated at an applied J-integral when the applied tearing modulus is less than the material tearing modulus. Alternately, the applied J-integral is less than the J-integral at the point of instability.

To complete the EPFM analysis, it must be shown that the applied J-integral is less than $J_{0.1}$, demonstrating that the crack driving force falls below the J-R curve at a crack extension of 0.1 inch.

3.0 ASSUMPTIONS

This section discusses assumptions and modeling simplifications applicable to the present evaluation of the DB-1 CRDM nozzle remnant flaw.

3.1 Unverified Assumptions

There are no assumptions that must be verified before the present analysis can be used to support the CRDM nozzle IDTB repair at Davis Besse Unit 1.

3.2 Justified Assumptions

The size of the J-groove weld prep and the thickness of the buttering are based on nominal dimensions. This is considered to be standard practice in stress analysis and fracture mechanics analysis. It is conservatively assumed that the postulated flaw extends through the entire J-groove weld and butter.

3.3 Modeling Simplifications

The finite element computer models used to generate residual stresses and transient operational stresses do not include the ID temper bead repair weld. This is deemed to be an appropriate modeling simplification considering the very local effect of the repair weld on stresses in the J-groove weld.

4.0 DESIGN INPUTS

This section provides basic input data needed to perform a fatigue crack growth analysis and a flaw evaluation of the final flaw size.

4.1 Materials

4.1.1 Mechanical and Thermal Properties

Table 4-1, Table 4-2, and Table 4-3 list the temperature dependent values of modulus of elasticity (E), Poisson's ratio (ν), and coefficient of thermal expansion (α) properties used in the finite element crack models. These properties are obtained from a previous stress analysis model of the Davis Besse CRDM nozzle and reactor vessel head [8]. Mechanical properties for the low alloy steel head are also provided in Table 4-1, where the flow stress is the average of the yield and ultimate strengths. The yield and ultimate strength values are obtained from Supplemental Requirements for SA-533 Manganese-Molybdenum-Nickel Alloy Steel Plates in the 1968 original construction code [9].

Component	Material
RV head	SA-533 Grade B Class 1 [2]
Cladding	Stainless steel (use Type 316 properties)
J-groove weld filler	Alloy 182 [2] (use Alloy 600 properties for SB-167)
J-groove weld butter	Alloy 182 [2] (use Alloy 600 properties for SB-167)

Table 4-1: Material Properties for Head

Component	Head					
Material	SA-533 Grade B Class 1					
Temperature	E (10^6 psi)	ν	α (10^{-6} in./in./°F)	σ_y (ksi)	σ_u (ksi)	σ_f (ksi)
70	29.00	0.29	7.06	50.00	80.00	65.00
100	29.00	0.29	7.06	50.00	80.00	65.00
200	28.50	0.29	7.34	47.15	76.45	61.80
300	28.00	0.29	7.43	45.25	76.40	60.83
400	27.40	0.29	7.58	44.50	76.40	60.45
500	27.00	0.29	7.70	43.20	76.40	59.80
600	26.40	0.29	7.83	42.00	76.40	59.20
700	25.30	0.29	7.94	40.60	76.40	58.50

Table 4-2: Material Properties for Weld Metal

Component	Weld Butter and Weld Filler		
Material	Use Alloy 600 (SB-167)		
Temperature	E (10^6 psi)	ν	α (10^{-6} in./in./°F)
70	30.82	0.3	6.90
100	30.82	0.3	6.90
200	30.20	0.3	7.20
300	29.90	0.3	7.40
400	29.50	0.3	7.57
500	29.00	0.3	7.70
600	28.70	0.3	7.82
700	28.20	0.3	7.94

Table 4-3: Material Properties for Cladding

Component	Cladding		
Material	Use Type 316 (16Cr-12Ni-2Mo) Stainless Steel		
Temperature	E (10^6 psi)	ν	α (10^{-6} in./in./°F)
70	28.14	0.3	8.54
100	28.14	0.3	8.54
200	27.60	0.3	8.76
300	27.00	0.3	8.97
400	26.50	0.3	9.21
500	25.80	0.3	9.42
600	25.30	0.3	9.60
700	24.80	0.3	9.76

4.1.2 Reference Temperature

Based on a highest measured RT_{NDT} of { }, a value of { } °F will be used as a conservative estimate of the RT_{NDT} for the SA-533, Grade B, Class 1 low alloy steel head material.

4.1.3 Fracture Toughness

From Article A-4200 of Section XI [11], the lower bound K_{Ia} fracture toughness for crack arrest can be expressed as

$$K_{Ia} = 26.8 + 12.445 \exp [\, 0.0145 \, (T - RT_{NDT}) \,],$$

where T is the crack tip temperature, RT_{NDT} is the reference nil-ductility temperature of the material, K_{Ia} is in units of ksi√in, and T and RT_{NDT} are in units of °F. In the present flaw evaluations, K_{Ia} is limited to a maximum value of 200 ksi√in (upper-shelf fracture toughness). Using the above equation with an RT_{NDT} of { } °F, K_{Ia} equals 200 ksi√in at a crack tip temperature of { } °F.

A higher measure of fracture toughness is provided by the K_{Ic} fracture toughness for crack initiation, approximated in Article A-4200 of Section XI [11] by

$$K_{Ic} = 33.2 + 20.734 \exp [\, 0.02 \, (T - RT_{NDT}) \,].$$

4.1.4 J-integral Resistance Curve

The J-integral resistance (J-R) curve, needed for the EPFM method of analysis, is obtained from the following power law expression for nuclear reactor pressure vessel steels [12],

$$J_R = C(\Delta a)^m,$$

where the coefficient, C, and exponent, m, depend on the Charpy V-notch upper-shelf energy, CVN, and the flow stress, σ_o or σ_f, as shown in Figure 4-1 and Figure 4-2.

An estimated value of the Charpy V-notch upper-shelf energy is available from a generic study of plate materials used in B&W fabricated reactor vessels [13]. This statistical analysis of { } determined with a 95% confidence that at least 95% of the population exhibited upper-shelf energies exceeding a lower tolerance value of { } ft-lbs in the transverse (weak) direction.

Using the above referenced Charpy V-notch upper-shelf energy correlation for the J-integral resistance curve with a Charpy V-notch upper-shelf energy of { } ft-lbs, the coefficients of the power law are found to be:

C = { }

m = { }

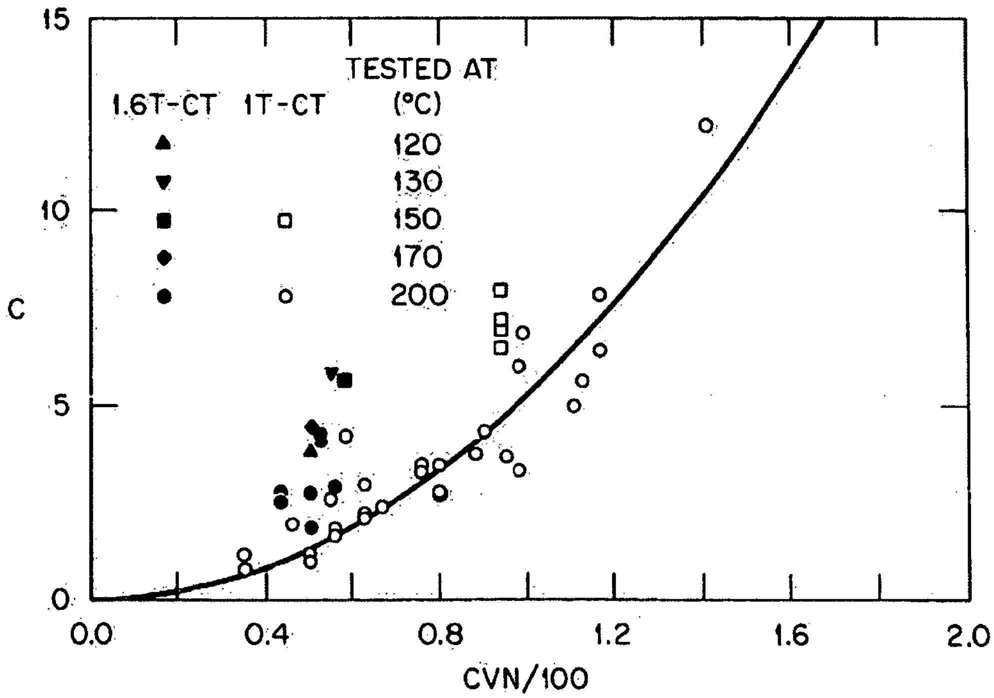

Figure 4-1: Correlation of Coefficient, C, of Power Law with Charpy V-Notch Upper Shelf Energy

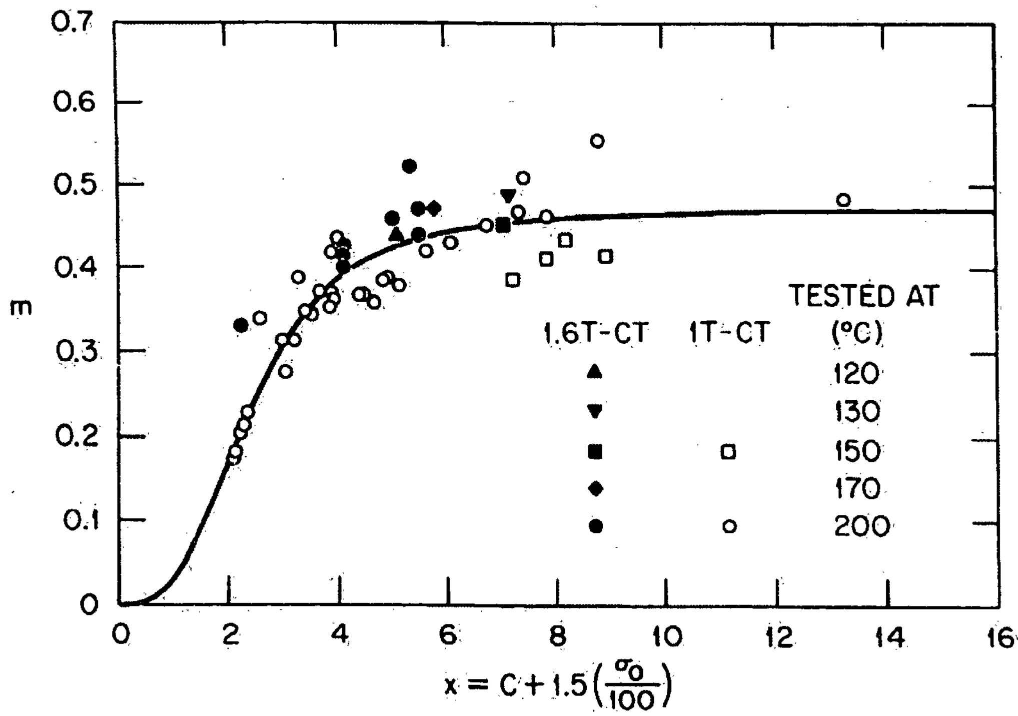

Figure 4-2: Correlation of Exponent, m, of Power Law with Coefficient, C, and Flow Stress, σ_o

4.1.5 Fatigue Crack Growth Rate

Flaw growth due to cyclic loading is calculated using the fatigue crack growth rate model from Article A-4300 of Section XI [11],

$$\frac{da}{dN} = C_o (\Delta K_I)^n,$$

where ΔK_I is the stress intensity factor range in ksi$\sqrt{\text{in}}$ and da/dN is in inches/cycle. The crack growth rates for a surface flaw will be used for the evaluation of the corner crack since it is assumed that the degraded condition of the J-groove weld and butter exposes the low alloy steel head material to the primary water environment.

The following equations from Section XI [11] are used to model fatigue crack growth.

$$\Delta KI = KI_{max} - KI_{min}$$
$$R = KI_{min} / KI_{max}$$

$0 \le R \le 0.25$: $\Delta K_I < 17.74$,

$$n = 5.95$$
$$C_o = 1.02 \times 10^{-12} \times S$$
$$S = 1.0$$

$\Delta K_I \ge 17.74$,

$$n = 1.95$$
$$C_o = 1.01 \times 10^{-7} \times S$$
$$S = 1.0$$

$0.25 \le R \le 0.65$: $\Delta K_I < 17.74\,[\,(3.75R + 0.06) / (26.9R - 5.725)\,]^{0.25}$,

$$n = 5.95$$
$$C_o = 1.02 \times 10^{-12} \times S$$
$$S = 26.9R - 5.725$$

$\Delta K_I \ge 17.74\,[\,(3.75R + 0.06) / (26.9R - 5.725)\,]^{0.25}$,

$$n = 1.95$$
$$C_o = 1.01 \times 10^{-7} \times S$$
$$S = 3.75R + 0.06$$

$0.65 \le R < 1.0$: $\Delta K_I < 12.04$,

$$n = 5.95$$
$$C_o = 1.02 \times 10^{-12} \times S$$
$$S = 11.76$$

$\Delta K_I \ge 12.04$,

$$n = 1.95$$
$$C_o = 1.01 \times 10^{-7} \times S$$
$$S = 2.5$$

4.2 Basic Geometry

The reactor vessel head and original CRDM nozzle penetration are described by the following key dimensions:

Radius to base metal	= {	} in. [14]
Head thickness (minimum)	= {	} in. [14]
Cladding thickness (nominal)	= {	} in. [15]
Butter thickness (nominal)	= {	} in. [16] or { }
Penetration bore	= {	} in. [16]
Penetration angle at outermost nozzle	= {	} deg. [16]

Details of the CRDM nozzle penetration and J-groove weld are provided in the description of the finite element crack model in Appendix C.

4.3 Operating Transients

The most significant normal and upset condition transients for fatigue crack growth may be combined into a 'full-range' transient comprised of heatup to 100% power (HU), a Type B reactor trip (RT), and subsequent normal cooldown (CD). Full-range transients are associated with operating events that include a zero state of stress. The reactor coolant functional specification [17] provides pressure and temperature time-histories for these transients, and lists 240 design cycles for the heatup/cooldown transient and { } cycles for the Type B reactor trip. The temperatures for these design transients have been modified to reflect a reactor coolant fluid temperature under the closure head of { } °F, based on a recent calculation to determine the DB-1 specific full load core exit temperature [18].

The rod withdrawal accident (RWA) upset transient was also selected since it experiences a high reactor coolant pressure of { } psig. This is especially significant for EPFM flaw evaluations where primary pressure loads are subjected to higher safety factors than secondary thermal loads. Since it is not expected that a rod withdrawal accident will occur during a four year period of operation, the RWA transient is not included in the calculation of fatigue crack growth, but it is addressed when evaluating the acceptability of the final flaw size. Transient 11 of the functional specification represents this design transient as an in-surge to the pressurizer which is based on the event that results in the greatest RCS pressure and temperature change. This event is initiated from 15% power and results in a 550 psi increase in RCS pressure and a 15 °F increase in temperature. The transient is of short duration, lasting approximately 20 to 30 seconds, producing only a minimal increase in head temperature. The functional specification transient bounds the expected change in the RCS pressure and temperature from the same event if initiated from full power conditions. As provided in Figure 15.2.2-1 of the DB-1 UFSAR [19], a rod withdrawal event from full power results in an increase of only 30 psi and 1.5 °F.

The functional specification also specifies one emergency condition transient, a stuck open turbine bypass valve, and two faulted condition transients, a steam line break and a loss of coolant accident. Appendix F of the Section III stress analysis for the CRDM nozzle IDTB weld repair [20] concludes that the stresses resulting from the emergency and faulted condition transients are bounded by those for the reactor trip transient. And since the safety factors on fracture toughness are higher for normal/upset conditions than for emergency/faulted conditions (Table 1-1), and the K_{Ic} fracture toughness for crack initiation is higher than the K_{Ia} fracture toughness for crack arrest (Section 4.1.3), it follows that the present flaw evaluations for normal/upset conditions also serve as a bounding analysis for emergency and faulted conditions. No further consideration of the emergency and faulted transients is therefore warranted.

4.4 Applied Stresses

Two sources of applied stress are considered for the present flaw evaluations, residual stresses from welding and stresses that occur during normal operation.

4.4.1 Residual Stresses

Residual stresses are obtained from a three-dimensional elastic-plastic finite element stress analysis performed by Dominion Engineering, Inc. [21]. Hoop stresses on the radial plane through the weld and butter are then mapped to the three-dimensional finite element crack model described in Section 2.1.1. Hoop stresses are used since these stresses are perpendicular to the crack face and therefore open the crack.

The DEI analysis simulated welding of the J-groove buttering, a post-weld heat treatment, welding of the J-groove partial penetration weld at the outmost CRDM nozzle, hydrostatic testing, operation at steady state temperature and pressure conditions, return to zero load conditions, removal of the original nozzle (Time 11006), and a second application of steady state loads. It is known from previous analysis that stresses at the outermost CRDM nozzle location conservatively bound stresses at all other nozzle locations [3]. The residual stresses in the remnant J-groove weld and butter are obtained from the load step corresponding to Time 11006, prior to the return to operating conditions

The DEI finite element model is shown in Figure 4-3, prior to removal of the CRDM nozzle. Figure 4-4 provides a closer view of the J-groove weld after the nozzle is removed.

4.4.2 Operational Stresses

Operational stresses are obtained by linear-elastic stress analysis using the three-dimensional finite element crack model described in Section 2.1.1, but with displacements normal to the crack face constrained to zero. Hoop stresses on a radial plane through the weld and butter are then copied directly to the crack model to facilitate the calculation of stress intensity factors along the entire crack front. Stresses are developed for the combined heatup/reactor trip/cooldown and rod withdrawal transients discussed in Section 4.3 using the thermal and structural finite element models described in Appendix D.

Figure 4-5 illustrates the "uncracked" finite element model used to calculate nodal temperatures (transient thermal analysis) and stresses (static stress analysis). The thermal phase of the solution is driven by wetted surface loads developed from time-dependent bulk fluid temperatures and convective heat transfer (film) coefficients. The structural model is then loaded by internal pressure (surface load) and nodal temperatures (body force loads from the thermal solution) to determine stresses at various times, as listed in Table 4-4. The critical time points are selected only after calculating stress intensity factors for each set of stresses output from the stress analysis solution. This process serves to maximize the stress intensity factors used in the fatigue crack growth analysis and the final flaw evaluations. The time points selected for use in the subsequent fracture mechanics analyses are identified in Table 4-4 by alphanumeric symbols.

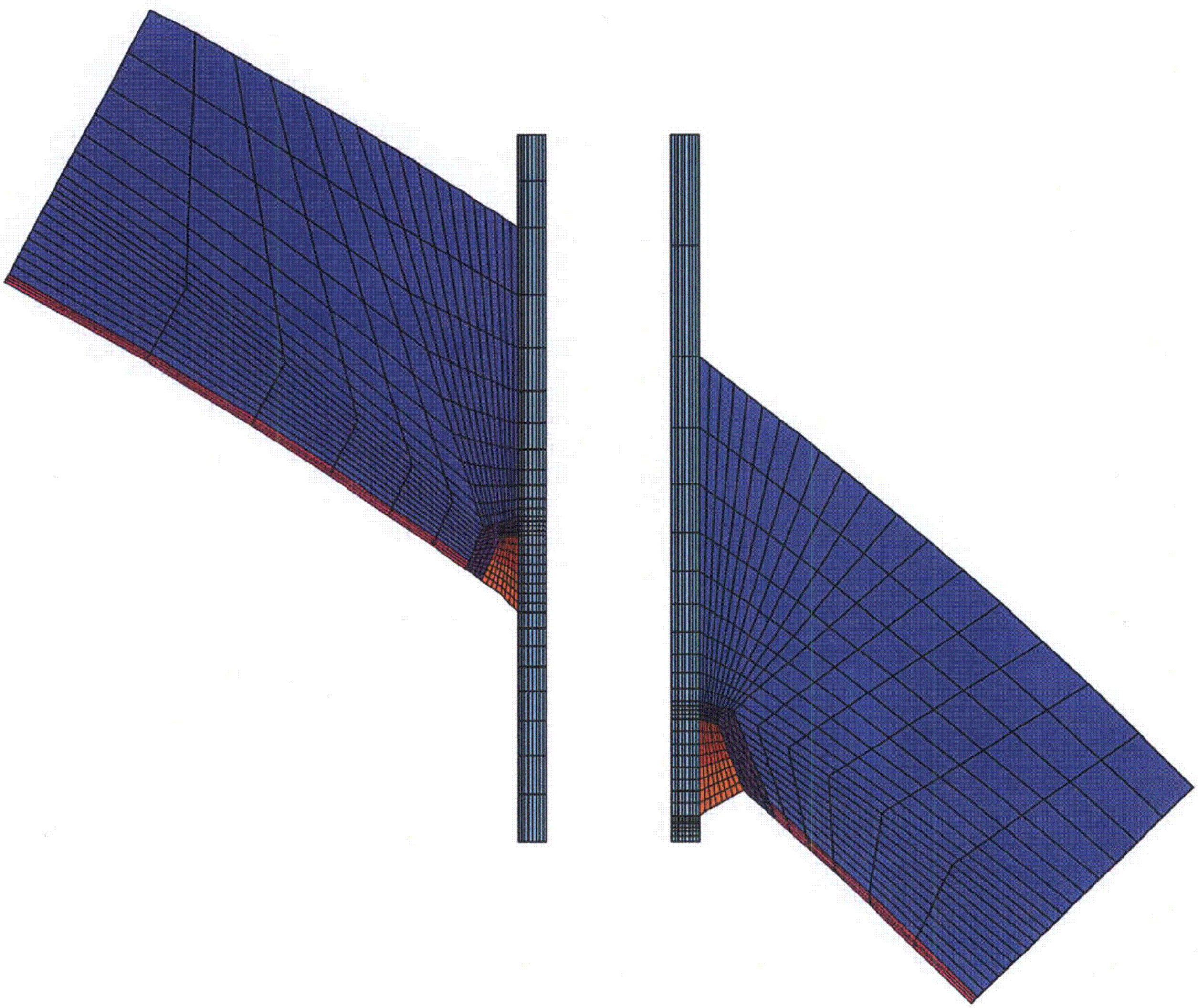

Figure 4-3: DEI Finite Element Stress Model

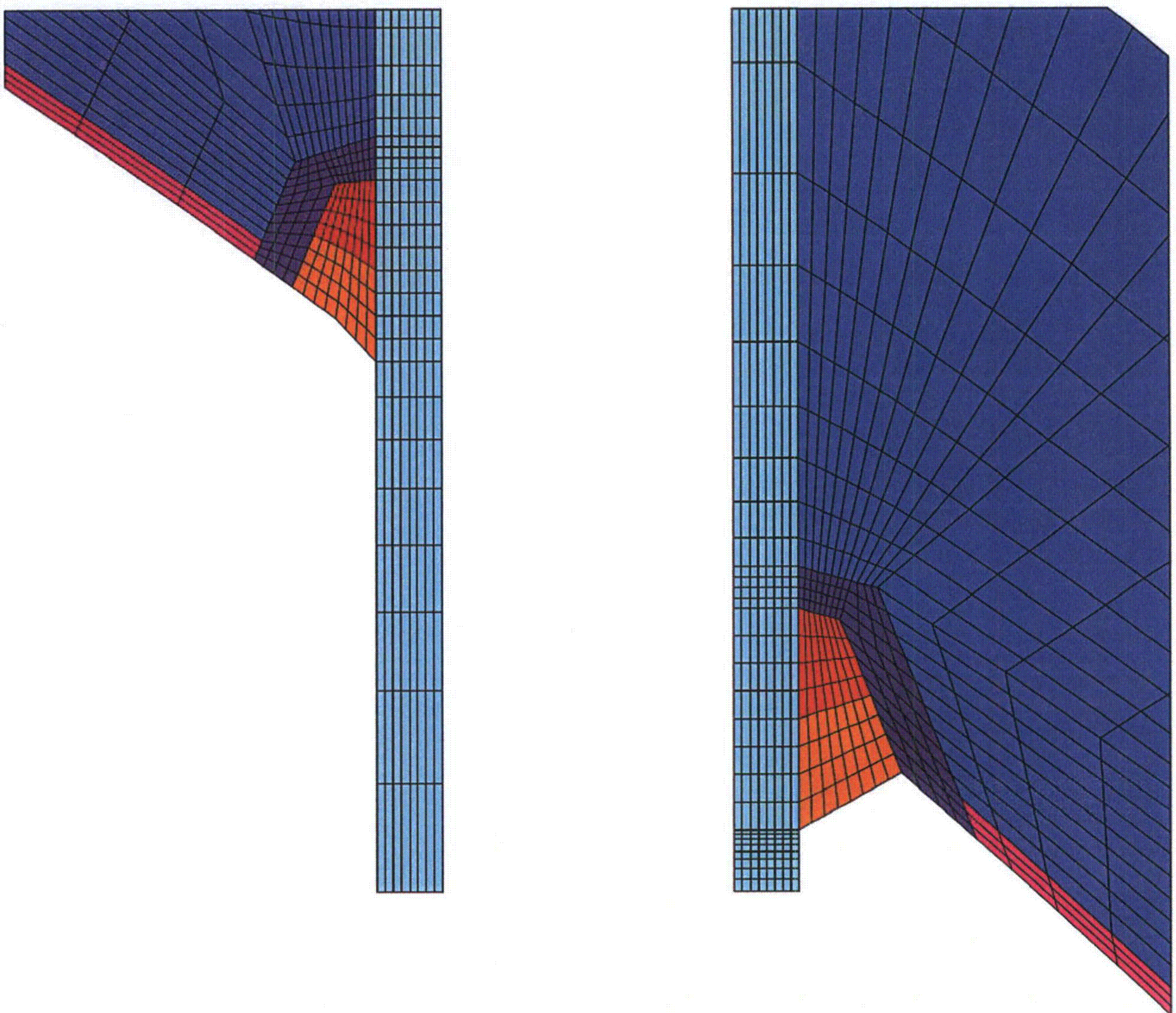

Figure 4-4: DEI Finite Element Stress Model – Weld Region

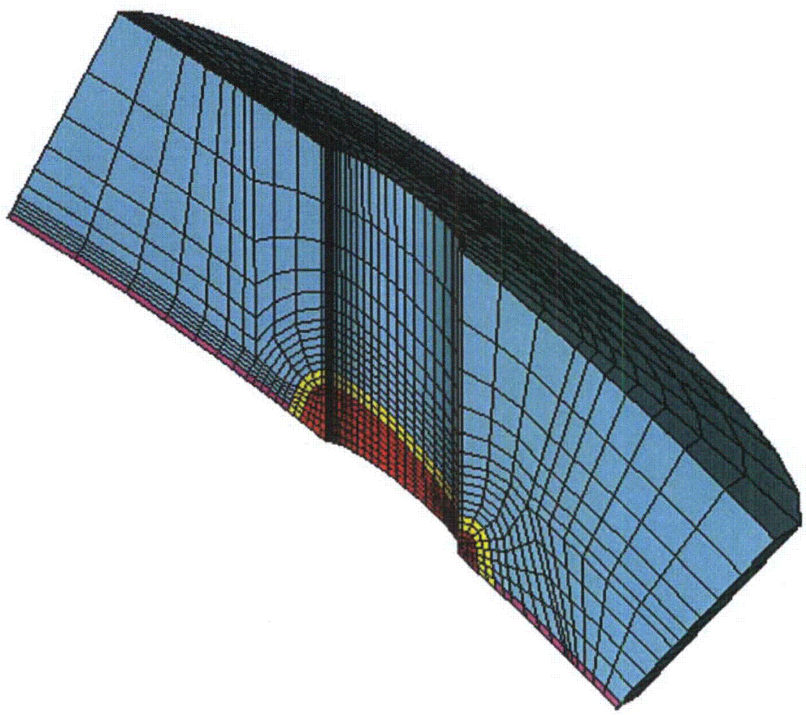

Figure 4-5: Finite Element Stress Model for Operational Stresses

Table 4-4: Transient Analysis Time Points for Operational Stresses

Symbol*	Load Step	Time (hours)	Temp. (F)	Pressure (psig)	Comment
Combined Heatup/Reactor Trip/Cooldown					
SD	1				Zero stress state
	2				End of heatup ramp
	3				After heatup ramp
	4				Steady state at 8% power
	5				End of power loading ramp (8%-100%)
	6				After power loading ramp (8%-100%)
SS	7				Steady state at 100% power
RT1	8				Reactor trip
	9				Reactor trip
	10				Reactor trip
	11				Reactor trip
	12				Reactor trip
RT2	13				Reactor trip
	14				Reactor trip
	15				Cooldown
	16				Cooldown
	17				Cooldown
	18				End of cooldown ramp
Rod Withdrawal Accident					
	1				
RWA	2				Maximum pressure
	3				
	4				

*Symbols:
SD = Shutdown
SS = Steady State
RT1 = Reactor Trip time 1
RT2 = Reactor Trip time 2
RWA = Rod Withdrawal Accident

5.0 CALCULATIONS

Propagation of a postulated initial flaw in the J-groove weld and butter is calculated to determine the final flaw size after a four year service interval. Flaw evaluations are then performed to assess the acceptability of the final flaw size.

5.1 Fatigue Crack Growth

Although it is believed that a PWSCC flaw would be confined to the J-groove weld and butter, it is postulated that a fatigue flaw would initiate in the low alloy steel head, combine with the PWSCC flaw, and propagate farther into the head under cyclic loads. Fatigue crack growth is calculated from stress intensity factors derived from a finite element crack model using residual stresses from a DEI stress analysis [21] and operational stresses calculated herein. The actual flaw growth calculations are presented in Table 5-1, along with a comparison of the final stress intensity factor with the LEFM acceptance criteria for each of the five significant load steps identified in Table 4-4. This table therefore serves several purposes; it determines the final flaw size at the end the designated service interval, it compares stress intensity factors at the final flaw size with LEFM acceptance criteria, and it serves as a means of identifying the controlling load steps for EPFM evaluation.

Crack growth is calculated for each heatup/cooldown cycle. Since the original design basis [17] specifies 240 heatup/cooldown cycles over a 40 year period, the corresponding time increment is one-sixth of a year.

Stress intensity factors are provided in Table 5-1 for all locations along the postulated crack front, including the cladding. It is apparent from the stress intensity factors listed in these tables for the initial flaw sizes that the highest value in the low alloy steel head occurs at the bored surface.

Table 5-1: Flaw Growth and LEFM Evaluation

INPUT DATA

Initial Flaw Size:	Depth along bore,	a_o =	2.035	in.
Fracture Toughness:	Reference temperature of head,	RTndt =	{ }	F
	Upper shelf toughness,	UST =	200	ksi√in

KIc = 33.2 + 20.734 exp [0.02 (T - RTndt)] ≤ UST
KIa = 26.8 + 12.445 exp [0.0145 (T - RTndt)] ≤ UST

Stress Intensity Factors:

	Condition*	SD	SS	RT1	RT2	RWA	
	Temperature	70	{ }	630	532	600	F
	Pressure	0	2155	2450	1720	2745	psig
	Sy	50.0	41.7	41.6	42.8	42.0	ksi
	KIc	58.5	200.0	200.0	200.0	200.0	ksi√in
	KIa	41.2	200.0	200.0	200.0	200.0	ksi√in
	Crack Front	Stress Intensity Factor, KI					
	Position	(psi√in)	(psi√in)	(psi√in)	(psi√in)	(psi√in)	
Cladding Surface	1	72012	93645	98490	126998	113102	
	2	57085	80022	85054	107657	98142	
	3	51528	76247	81503	101098	94057	
	4	50744	76792	82152	99156	94199	
	5	51092	77639	82959	97602	94399	
	6	50355	76403	81504	93813	92098	
	7	50354	76220	81039	89789	90395	
	8	55409	83992	89074	96389	98404	
	9	58477	93556	99531	107438	110130	
Bored Surface	10	61779	101703	108389	117216	120167	

* Condition	Description
SD	Time step 1 at 0 hr. of heatup/reactor trip/cooldown (shutdown w/ only residual stress)
SS	Time step 7 at 10.0000 hr. of heatup/reactor trip/cooldown (steady state at 100% power)
RT1	Time step 8 at 10.0028 hr. of heatup/reactor trip/cooldown (during reactor trip)
RT2	Time step 13 at 10.1184 hr. of heatup/reactor trip/cooldown (during reactor trip)
RWA	Time step 2 at 0.0044 hr. into rod withdrawal accident (high pressure condition)

Table 5-1: Flaw Growth and LEFM Evaluation (Cont'd)

FATIGUE CRACK GROWTH

Transient Description: 240 cycles over 40 years

$\Delta N =$ 6 cycles/year

			Crack Front Position 10						
Cycle	Operating Time (end of yr.)	a (in.)	RT2 KI(a)max (ksi√in)	SD KI(a)min (ksi√in)	ΔKI (ksi√in)	Δa (in.)	SS KI(a) (ksi√in)	RT1 KI(a) (ksi√in)	RWA KI(a) (ksi√in)
0	0.000	2.03500	117.216	61.779	55.437		101.703	108.389	120.167
1	0.167		117.305	61.826	55.479		101.781	108.472	120.259
2	0.333		117.395	61.873	55.522		101.858	108.554	120.350
3	0.500		117.484	61.920	55.564		101.936	108.637	120.442
4	0.667		117.574	61.968	55.606		102.013	108.720	120.534
5	0.833		117.663	62.015	55.649		102.091	108.803	120.626
6	1.000		117.753	62.062	55.691		102.169	108.885	120.717
7	1.167		117.843	62.109	55.733		102.247	108.968	120.809
8	1.333		117.932	62.157	55.776		102.325	109.051	120.901
9	1.500		118.022	62.204	55.818		102.403	109.135	120.994
10	1.667		118.112	62.251	55.861		102.481	109.218	121.086
11	1.833		118.202	62.299	55.903		102.559	109.301	121.178
12	2.000		118.292	62.346	55.946		102.637	109.384	121.270
13	2.167		118.382	62.394	55.989		102.715	109.467	121.363
14	2.333		118.472	62.441	56.031		102.793	109.551	121.455
15	2.500		118.563	62.489	56.074		102.871	109.634	121.548
16	2.667		118.653	62.536	56.117		102.950	109.718	121.640
17	2.833		118.743	62.584	56.159		103.028	109.801	121.733
18	3.000		118.834	62.632	56.202		103.107	109.885	121.826
19	3.167		118.924	62.679	56.245		103.185	109.969	121.918
20	3.333		119.015	62.727	56.288		103.264	110.052	122.011
21	3.500		119.106	62.775	56.331		103.342	110.136	122.104
22	3.667		119.196	62.823	56.374		103.421	110.220	122.197
23	3.833		119.287	62.871	56.416		103.500	110.304	122.290
24	4.000		119.378	62.918	56.459		103.579	110.388	122.383

Table 5-1: Flaw Growth and LEFM Evaluation (Cont'd)

LEFM FRACTURE TOUGHNESS MARGINS

Period of Operation: Time = 4 years

Flaw Size: a = { } in.

	Loading Conditions					
	SD	SS	RT1	RT2	RWA	
Fracture Toughness, KIc	58.5	200.0	200.0	200.0	200.0	ksi√in
Fracture Toughness, KIa	41.2	200.0	200.0	200.0	200.0	ksi√in
Position 10						
KI(a)	62.918	103.579	110.388	119.378	122.383	ksi√in
a_e	2.1948	2.4378	2.4847	2.5232	2.5612	in.
KI(a_e)	64.158	111.313	119.767	130.520	134.811	ksi√in
Margin = KIc / KI(a_e)	n/a	n/a	n/a	n/a	n/a	
Margin = KIa / KI(a_e)	0.64	1.80	1.67	1.53	1.48	

where: $ae = a + 1/(6\pi)\,[KI(a)/Sy]^2$

$KI(a_e) = KI(a)*\sqrt{(a_e/a)}$

5.2 LEFM Flaw Evaluations

The results of the linear-elastic fracture mechanics flaw evaluations are summarized below for the final size of the postulated flaw after fatigue crack growth.

Flaw Size

Initial flaw size,	a_i = 2.035 in.
Final flaw size after 4 years,	a_f = { } in.
Flaw growth,	Δa = { } in.

Controlling Transients	Shutdown	Heatup/Cooldown w/ Reactor Trip (RT2)	Rod Withdrawal Accident
Condition	Low Temperature	Normal	Upset
Temperature,	T = 70 °F	{ } °F	{ } °F
Fracture toughness,	K_{Ia} = 41.2 ksi√in	200.0 ksi√in	200.0 ksi√in
Final stress intensity factor,	$K_I(a_f)$ = 62.9 ksi√in	119.4 ksi√in	122.4 ksi√in
Effective flaw size,	a_e = 2.195 in.	2.523 in.	2.561 in.
Effective stress intensity factor,	$K_I(a_e)$ = 64.2 ksi√in	130.5 ksi√in	134.8 ksi√in
Fracture toughness margin (> 3.16),	K_{Ia} / $K_I(a_e)$ = 0.64	1.53	1.48

Since the controlling fracture toughness margins are less than the Code required minimums, EPFM flaw evaluations will be performed to account for the ductile behavior of the low alloy steel during stable crack growth.

5.3 EPFM Flaw Evaluations

The elastic-plastic fracture mechanics procedure described in Section 2.3 is used to evaluate the final size of the postulated flaw after fatigue crack growth.

Flaw Size

Initial flaw size, a_i = 2.035 in.

Final flaw size after 4 years, a_f = { } in.

Controlling Transients		Shutdown	Heatup/Cooldown w/ Reactor Trip (RT2)	Rod Withdrawal Accident
SCREENING PROCEDURE				
	T =	70 °F	{ } °F	{ } °F
	E =	29000 ksi	26808 ksi	26400 ksi
	ν =	0.3	0.3	0.3
	$E' = E/(1-\nu^2)$ =	31860 ksi	29450 ksi	29010 ksi
	σ_y =	50.0 ksi	42.8 ksi	42.0 ksi
	σ_u =	80.0 ksi	76.4 ksi	76.4 ksi
	σ_f =	65.0 ksi	59.6 ksi	59.2 ksi
Crack initiation toughness,	K_{Ic} =	58.5 ksi√in	200.0 ksi√in	200.0 ksi√in
Total applied K_I,	$K_I(a_e)$ =	64.2 ksi√in	130.5 ksi√in	134.8 ksi√in
Then,	$K_r' = K_I(a_e) / K_{Ic}$ =	1.096	0.653	0.674

From finite element stress analysis, the maximum crack face stresses due to residual stress, pressure, and thermal gradients are

		Shutdown	Heatup/Cooldown w/ Reactor Trip (RT2)	Rod Withdrawal Accident
	σ_{max} =	66.4 ksi	114.6 ksi	114.5 ksi
Then,	$S_r' = \sigma_{max} / \sigma_f$ =	1.022	1.923	1.934
Screening ratio,	K_r' / S_r' =	1.073	0.339	0.349

The analysis is therefore in the EPFM regime ($1.8 > K_r' / S_r' \geq 0.2$) for both loading conditions.

EPFM ANALYSIS

		Shutdown	Heatup/Cooldown w/ Reactor Trip (RT2)	Rod Withdrawal Accident
Total applied K_I,	$K_I(a)$ =	62.9 ksi√in	119.4 ksi√in	122.4 ksi√in
K_I primary (pressure from Appendix E),	$K_{Ip}(a)$ =	0.0 ksi√in	39.9 ksi√in	63.7 ksi√in
K_I secondary (residual plus thermal),	$K_{Is}(a)$ =	62.9 ksi√in	79.5 ksi√in	58.7 ksi√in
Multiplying by $\sqrt{(a_e/a)}$,	$K'_{Ip}(a)$ =	0.0 ksi√in	43.6 ksi√in	70.2 ksi√in
	$K'_{Is}(a)$ =	64.2 ksi√in	86.9 ksi√in	64.7 ksi√in

Table 5-2, Table 5-3, and Table 5-4 develop all the data necessary to construct J-T diagrams for the controlling operating conditions. The J-T diagrams are presented in Figure 5-1, Figure 5-2, and Figure 5-3.

For shutdown conditions, Table 5-2 shows for an applied J-integral of 0.291 kips/in, corresponding to safety factors of 3 and 1.5, the applied tearing modulus, 0.945, is less than the material tearing modulus, 317.0, indicating flaw stability. Alternately, the applied J-integral is less than the J-integral, 3.415 kips/in, at the point of instability. For safety factors of 1.5 and 1, the applied J-integral of 0.129 kips/in is less than the $J_{0.1}$ value of 1.350 kips/in, demonstrating that the crack driving force falls below the J-R curve at a crack extension of 0.1 inch.

For the heatup/cooldown transient with reactor trip, Table 5-3 shows for an applied J-integral of 2.317 kips/in, corresponding to safety factors of 3 and 1.5, the applied tearing modulus, 8.283, is less than the material tearing modulus, 20.69, indicating flaw stability. Alternately, the applied J-integral is less than the J-integral, 3.402 kips/in, at the point of instability. For safety factors of 1.5 and 1, the applied J-integral of 0.788 kips/in is less than the $J_{0.1}$ value of 1.363 kips/in, demonstrating that the crack driving force falls below the J-R curve at a crack extension of 0.1 inch.

For rod withdrawal accident conditions, Table 5-4 shows for an applied J-integral of 3.258 kips/in, corresponding to safety factors of 3 and 1.5, the applied tearing modulus, 11.63, is less than the material tearing modulus, 12.88, indicating flaw stability. Alternately, the applied J-integral is less than the J-integral, 3.401 kips/in, at the point of instability. For safety factors of 1.5 and 1, the applied J-integral of 0.995 kips/in is less than the $J_{0.1}$ value of 1.364 kips/in, demonstrating that the crack driving force falls below the J-R curve at a crack extension of 0.1 inch.

Table 5-2: EPFM Evaluation for Shutdown Conditions

EPFM Equations:

$J_{mat} = C(\Delta a)^m$ C = { }

$T_{mat} = (E/\sigma_f^2)*Cm(\Delta a)^{m-1}$ m = { }

$J_{app} = (SF_p*K'_{Ip}+SF_s*K'_{Is})^2/E'$

$T_{app} = (E/\sigma_f^2)*(dJ_{app}/da)$

Ductile Crack Growth Stability Criterion: $T_{app} < T_{mat}$

At instability: $T_{app} = T_{mat}$

Safety Factors		SF*K'$_{Ip}$	SF*K'$_{Is}$	J_{app}	T_{app}	Stable?
Primary	Secondary	(ksi√in)	(ksi√in)	(kips/in)		
1.00	1.00	0.000	64.158	0.129	0.420	Yes
2.00	2.00	0.000	128.316	0.517	1.681	Yes
3.00	1.50	0.000	96.237	0.291	0.945	Yes
5.00	5.00	0.000	320.791	3.230	10.503	Yes
7.00	7.00	0.000	449.108	6.331	20.587	No

Iterate on safety factor until $T_{app} = T_{mat}$ to determine $J_{instability}$:

				$J_{instability}$	T_{app}	T_{mat}
5.1412	5.1412	0.000	329.852	3.415	11.105	11.105

at J_{mat} = 0.291 kips/in, T_{mat} = 316.734

Applied J-Integral Criterion: $J_{app} < J_{0.1}$

where, $J_{0.1} = J_{mat}$ at Δa = 0.1 in.

Safety Factors		SF*K'$_{Ip}$	SF*K'$_{Is}$	J_{app}	$J_{0.1}$	OK?
Primary	Secondary	(ksi√in)	(ksi√in)	(kips/in)	(kips/in)	
1.50	1.00	0.000	64.158	0.129	1.350	Yes

Table 5-3: EPFM Evaluation for Heatup/Cooldown with Reactor Trip

EPFM Equations:

$$J_{mat} = C(\Delta a)^m$$
$$T_{mat} = (E/\sigma_f^2)*Cm(\Delta a)^{m-1}$$

C = { }
m = { }

$$J_{app} = (SF_p*K'_{Ip}+SF_s*K'_{Is})^2/E'$$
$$T_{app} = (E/\sigma_f^2)*(dJ_{app}/da)$$

Ductile Crack Growth Stability Criterion: $T_{app} < T_{mat}$

At instability: $T_{app} = T_{mat}$

Safety Factors		$SF*K'_{Ip}$	$SF*K'_{Is}$	J_{app}	T_{app}	Stable?
Primary	Secondary	(ksi√in)	(ksi√in)	(kips/in)		
1.00	1.00	43.630	86.890	0.578	2.068	Yes
2.00	1.00	87.261	86.890	1.030	3.681	Yes
3.00	1.50	130.891	130.335	2.317	8.283	Yes
5.00	1.00	218.152	86.890	3.160	11.294	Yes
7.00	1.00	305.412	86.890	5.226	18.680	No

Iterate on safety factor until $T_{app} = T_{mat}$ to determine $J_{instability}$:

				$J_{instability}$	T_{app}	T_{mat}
2.4252	2.4252	105.812	210.726	3.402	12.161	12.161

at J_{mat} = 2.317 kips/in, T_{mat} = 20.694

Applied J-Integral Criterion: $J_{app} < J_{0.1}$

where, $J_{0.1} = J_{mat}$ at Δa = 0.1 in.

Safety Factors		$SF*K'_{Ip}$	$SF*K'_{Is}$	J_{app}	$J_{0.1}$	OK?
Primary	Secondary	(ksi√in)	(ksi√in)	(kips/in)	(kips/in)	
1.50	1.00	65.445	86.890	0.788	1.363	Yes

Table 5-4: EPFM Evaluation for Rod Withdrawal Accident

EPFM Equations:

$J_{mat} = C(\Delta a)^m$ C = { }

$T_{mat} = (E/\sigma_f^2)*Cm(\Delta a)^{m-1}$ m = { }

$J_{app} = (SF_p*K'_{Ip}+SF_s*K'_{Is})^2/E'$

$T_{app} = (E/\sigma_f^2)*(dJ_{app}/da)$

Ductile Crack Growth Stability Criterion: $T_{app} < T_{mat}$

At instability: $T_{app} = T_{mat}$

Safety Factors		SF*K'$_{Ip}$	SF*K'$_{Is}$	J_{app}	T_{app}	Stable?
Primary	Secondary	(ksi√in)	(ksi√in)	(kips/in)		
1.00	1.00	70.154	64.657	0.626	2.236	Yes
2.00	1.00	140.308	64.657	1.448	5.168	Yes
3.00	1.50	210.461	96.986	3.258	11.628	Yes
5.00	1.00	350.769	64.657	5.949	21.231	No
7.00	1.00	491.076	64.657	10.646	37.993	No

Iterate on safety factor until $T_{app} = T_{mat}$ to determine $J_{instability}$:

				$J_{instability}$	T_{app}	T_{mat}
2.3301	2.3301	163.463	150.656	3.401	12.138	12.138

at J_{mat} = 3.258 kips/in, T_{mat} = 12.883

Applied J-Integral Criterion: $J_{app} < J_{0.1}$

where, $J_{0.1} = J_{mat}$ at Δa = 0.1 in.

Safety Factors		SF*K'$_{Ip}$	SF*K'$_{Is}$	J_{app}	$J_{0.1}$	OK?
Primary	Secondary	(ksi√in)	(ksi√in)	(kips/in)	(kips/in)	
1.50	1.00	105.231	64.657	0.995	1.364	Yes

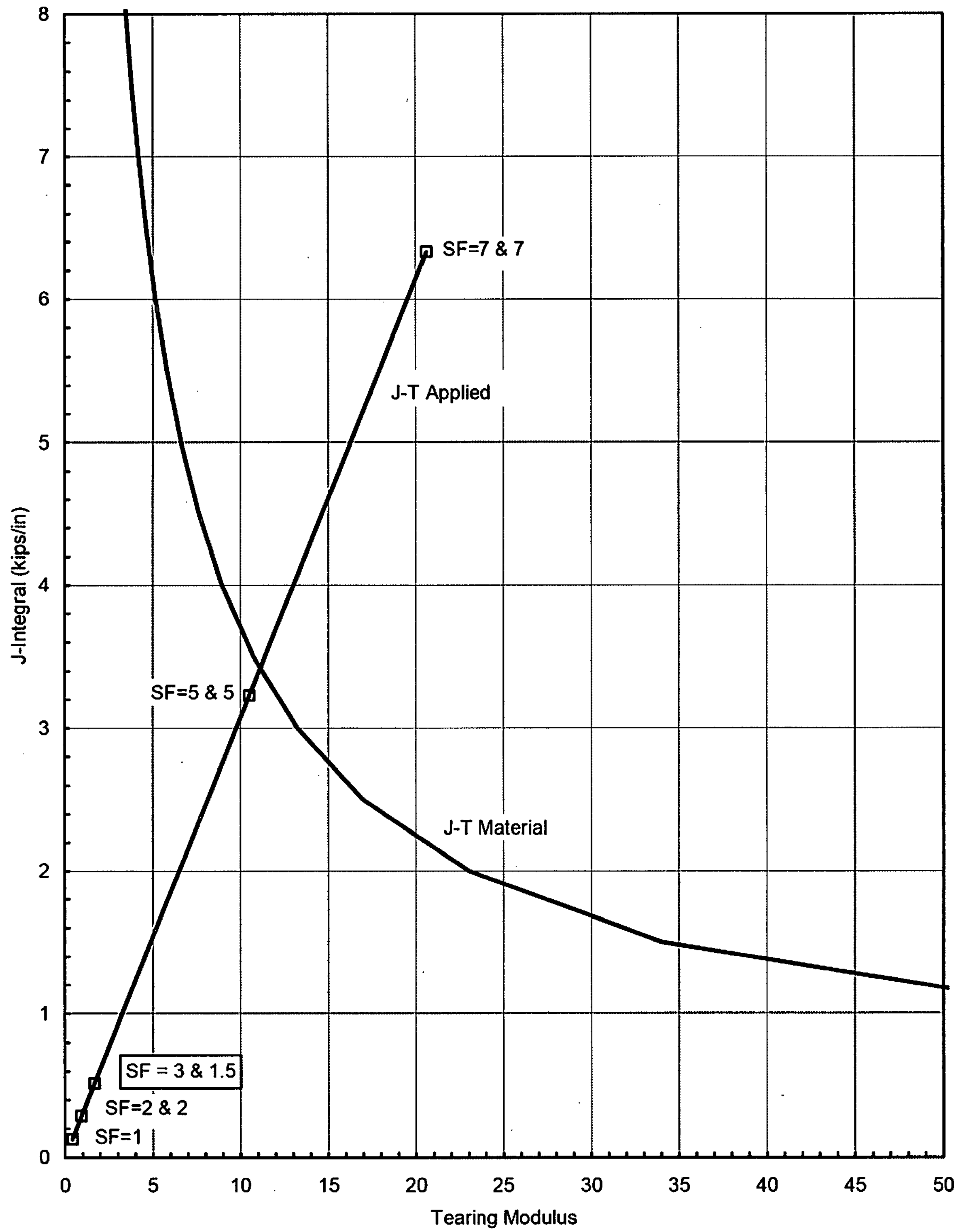

Figure 5-1: J-T Diagram for Shutdown Conditions

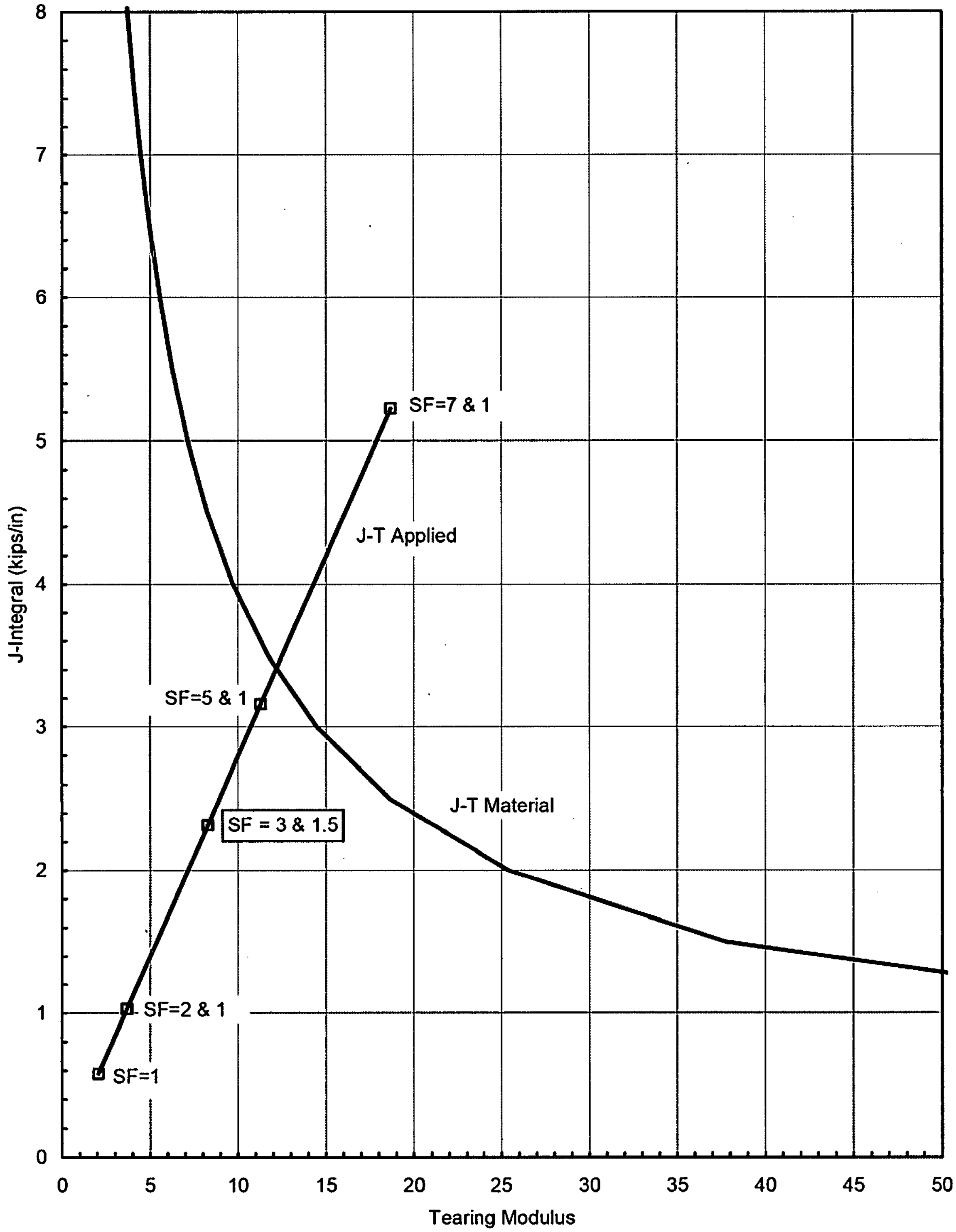

Figure 5-2: J-T Diagram for Heatup/Cooldown with Reactor Trip

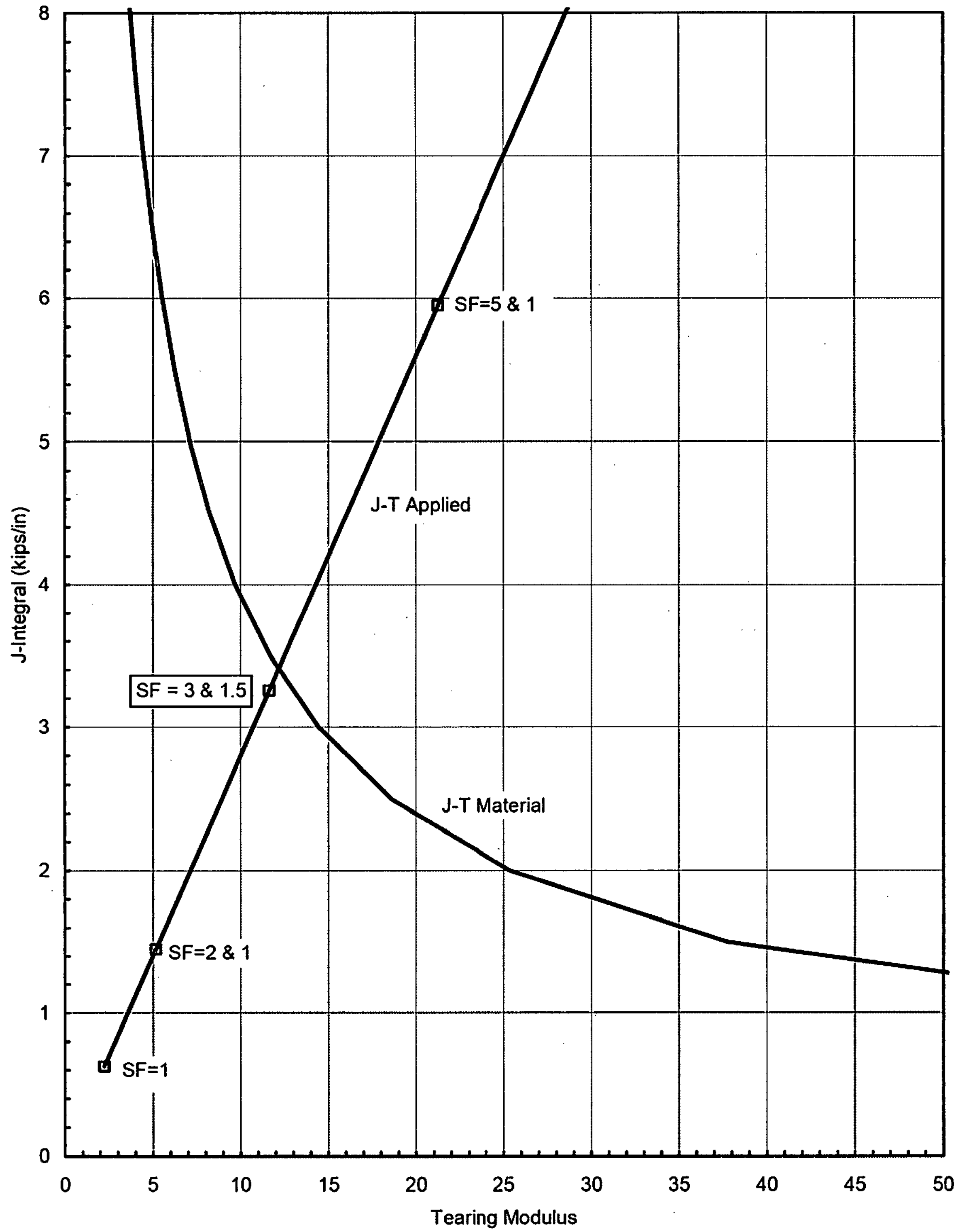

Figure 5-3: J-T Diagram for Rod Withdrawal Accident

6.0 SUMMARY OF RESULTS AND CONCLUSIONS

Elastic-plastic fracture mechanics has been used to evaluate a postulated radial flaw in the J-groove weld and butter of an outermost CRDM nozzle reactor vessel head penetration. The final flaw size was determined by linear elastic fracture mechanics for 4 years of fatigue crack growth.

6.1 Summary of Results

Flaw Size

Initial flaw size,	a_i = 2.035 in.
Final flaw size after 4 years,	a_f = { } in.

Controlling Transients	Shutdown	Heatup/Cooldown w/ Reactor Trip	Rod Withdrawal Accident
Temperature,	T = 70 °F	{ }°F	{ }°F
Safety factors (primary/secondary),	SF = 3 / 1.5	3 / 1.5	3 / 1.5
Material tearing modulus,	T_{mat} = 317.0	20.69	12.88
Applied tearing modulus (< T_{mat})	T_{app} = 0.945	8.283	11.63
Safety factors (primary/secondary),	SF = 1.5 / 1	1.5 / 1	1.5 / 1
Material J-integral,	$J_{0.1}$ = 1.350 kips/in	1.363 kips/in	1.364 kips/in
Applied J-integral (< $J_{0.1}$)	J_{app} = 0.129 kips/in	0.788 kips/in	0.995 kips/in

6.2 Conclusion

Based on a combination of linear elastic and elastic plastic fracture mechanics analysis of a postulated remaining flaw in the original Alloy 182 J-groove weld and butter material, a Davis Besse Unit 1 CRDM nozzle is considered to be acceptable for at least 4 years of operation following an IDTB weld repair.

7.0 REFERENCES

1. AREVA NP Drawing 02-9134305-004, "Davis Besse CRDM Nozzle ID Temper Bead Weld Repair."
2. AREVA NP Document 08-9134304-000, "Davis Besse RVCH CRDM Penetration Modification," March 2010.
3. AREVA NP Document 38-1288564-00, "Calculation Number C-3206-00-1, Rev. 0, Davis Besse CRDM Stress Analysis," December 2001.
4. AREVA NP Document 51-5012047-00, "Stress Corrosion Cracking of Low Alloy Steel," March 2001.
5. AREVA NP Document 32-9066059-000, "Watts Bar CRDM Nozzle IDTB J-Groove Weld Analysis," December 2007.
6. ANSYS Finite Element Computer Code, Version 10.0, ANSYS Inc., Canonsburg, PA.
7. T.L. Anderson, Fracture Mechanics: Fundamentals and Applications, CRC Press, 1991.
8. AREVA NP Document 32-5011864-07, "CRDMH Connection 3D FE Model," March 2001.
9. ASME Boiler and Pressure Vessel Code, Section II, Material Specifications: Part A - Ferrous, 1965 Edition with Summer 1968 Addendum.
10. BAW-10046A, Rev. 2, "Methods of Compliance With Fracture Toughness and Operational Requirements of 10 CFR 50, Appendix G," B&W Owners Group Materials Committee Topical Report, June 1986.
11. ASME Boiler and Pressure Vessel Code, Section XI, Rules for Inservice Inspection of Nuclear Power Plant Components, 1995 Edition with Addenda through 1996.
12. NUREG-0744, Vol. 2, Rev. 1, "Resolution of the Task A-11 Reactor Vessel Materials Toughness Safety Issue," Appendix D, Materials Toughness Properties, Division of Safety Technology, Office of Nuclear Reactor Regulation, U.S. Nuclear Regulatory Commission, Washington, D.C. 20555, October 1982.
13. AREVA NP Document 77-2313-006 (BAW-2313, Revision 6), "B&W Fabricated Reactor Vessel Materials and Surveillance Data Information," AREVA NP Inc., November 2008.
14. AREVA NP Drawing 02-142178E-05, "Closure Head Center Disc." (DB-1 Midland Head)
15. AREVA NP Drawing 02-154613E-08, "Arrangement Reactor Vessel Longitudinal Section." (DB-1 Midland Head)

16. AREVA NP Drawing 02-142179E-10, "Closure Head Sub-Assembly." (DB-1 Midland Head)

17. AREVA NP Document 18-1149327-003, "Functional Specification for Reactor Coolant System for Davis-Besse," July 2008.

18. AREVA NP Document 51-9137401-000, "Evaluation of Fluid Temperature in DB RV Closure Head," May 2010.

19. * Davis-Besse Nuclear Power Station No. 1 Updated Safety Analysis Report, Revision 26, June 2008.

20. AREVA NP Document 32-5012424-12, "CRDM Temper Bead Bore Weld Analysis," April 2004.

21. AREVA NP Document 32-9134665-001, "DEI Residual Stress Analysis for DB-1 CRDM Nozzle IDTB Repair," DEI Calc. No. C-8616-00-01, Rev. 1, Davis Besse CRDM Nozzle Welding Residual Stress Analysis, May 2010.

* Reference 19 is not retrievable from the AREVA NP Records Management system but are referenced here in accordance with AREVA NP Procedure 0402-01, Attachment 8. This customer reference is a valid source of design input as authorized by the Project Manager signature on page 2.

APPENDIX A: VERIFICATION OF COMPUTER CODE ANSYS

The ANSYS finite element computer program [6] is verified for use in the present flaw evaluation by executing three test cases from the ANSYS set of verification problems that utilize the SOLID90 thermal and SOLID95 structural 20-node 3-D solid elements. Test case VM161 determines heat flow in an insulated pipe. Test case VM148 analyzes a cantilevered, parabolic beam subjected to a static bending load. Test case VM143 calculates a stress intensity factor for a crack in a plate. All three test cases executed properly, as demonstrated below.

Verification Problem VM161

Thermal Analysis of an Insulated Pipe

File: vm161.vrt

VM161 RESULTS COMPARISON

Surface Heat Flow Rate

	TARGET	ANSYS	RATIO
q (BTU/hr)	362.0	362.0	1.000

Verification Problem VM148

Bending of a Parabolic Beam

File: vm148.vrt

VM148 RESULTS COMPARISON

End Displacement

	TARGET	ANSYS	RATIO
Y Deflection (in.)	-0.01067	-0.01062	0.995

Verification Problem VM143

Fracture Mechanics Analysis of a Crack in a Plate

File: vm143.vrt

VM143 RESULTS COMPARISON

Stress Intensity Factor by Displacement Extrapolation

	TARGET	ANSYS	RATIO
3-D ANALYSIS	1.0249	1.0620	1.036

APPENDIX B: COMPUTER FILES IN COLDSTOR

The computer files listed below, which are unchanged from those listed in document 32-9134664-003, are stored in the AREVA NP COLDStor repository in directory "\cold\41304\32-9134664-003\official".

ANSYS Models

File Name	Description	Modified Date	Installed Date
Uphill_Crack_Model.db	Crack model for uphill J-groove weld	03-19-10	05-07-10
Uphill_UnCrack_Model.db	Model for calculating operating stresses	03-20-10	05-07-10
MatlAndMesh.dat	Material data for thermal and stress analysis	04-04-10	05-07-10

ANSYS Thermal Analysis

File Name	Description	Modified Date	Installed Date
HU_RX8B_Thermal.dat	Input file for HU/RT/CD thermal analysis	05-03-10	05-07-10
HU_RX8B_Thermal.out	Output file for HU/RT/CD thermal analysis	05-03-10	05-07-10
RWA_Thermal.dat	Input file for RWA thermal analysis	04-05-10	05-07-10
RWA_Thermal.out	Output file for RWA thermal analysis	04-05-10	05-07-10

ANSYS Stress Analysis

File Name	Description	Modified Date	Installed Date
HU_RX8B_Stress.dat	Input file for HU/RT/CD stress analysis	05-04-10	05-07-10
HU_RX8B_Stress.out	Output file for HU/RT/CD stress analysis	05-04-10	05-07-10
RWA_Stress.dat	Input file for RWA stress analysis	04-04-10	05-07-10
RWA_Stress.out	Output file for RWA stress analysis	04-05-10	05-07-10

ANSYS Macros for Transferring Stresses to Crack Model

File Name	Description	Modified Date	Installed Date
Format_Stresses_Driver.mac	Driver to get residual stresses	03-28-10	05-07-10
Format_Stresses.mac	Macro to get residual stresses	03-28-10	05-07-10
Get_Stresses_Driver.mac	Driver to get operating stresses	05-04-10	05-07-10

File Name	Description	Modified Date	Installed Date
Get_Stresses.mac	Macro to get operating stresses	04-05-10	05-07-10

ANSYS Analysis to Calculate Stress Intensity Factors (SIF)

File Name	Description	Modified Date	Installed Date
Uphill_Crack_Pressure.inp	Input file for pressure loading	03-23-10	05-07-10
Press_Up.output	Output file for pressure loading	04-07-10	05-07-10
Get_RESI_SIFs.mac	Macro to get SIFs for residual stresses	04-08-10	05-07-10
Get_HUCD_SIFs.mac	Macro to get SIFs for HU/RT/CD stresses	05-04-10	05-07-10
Get_RWA_SIFs.mac	Macro to get SIFs for RWA stresses	04-05-10	05-07-10
Map_Stresses_Up.mac	Macro to map stresses from uncracked model to crack model	03-24-10	05-07-10
PrtKlup.mac	Macro to write SIFs to output file	03-24-10	05-07-10
RESIu.output	Output file for residual SIFs	04-08-10	05-07-10
HUCDu1.output	Output file for HU/RT/CD SIFs (load step 1)	05-04-10	05-07-10
HUCDu2.output	Output file for HU/RT/CD SIFs (load step 2)	05-04-10	05-07-10
HUCDu3.output	Output file for HU/RT/CD SIFs (load step 3)	05-04-10	05-07-10
HUCDu4.output	Output file for HU/RT/CD SIFs (load step 4)	05-04-10	05-07-10
HUCDu5.output	Output file for HU/RT/CD SIFs (load step 5)	05-04-10	05-07-10
HUCDu6.output	Output file for HU/RT/CD SIFs (load step 6)	05-04-10	05-07-10
HUCDu7.output	Output file for HU/RT/CD SIFs (load step 7)	05-04-10	05-07-10
HUCDu8.output	Output file for HU/RT/CD SIFs (load step 8)	05-04-10	05-07-10
HUCDu9.output	Output file for HU/RT/CD SIFs (load step 9)	05-04-10	05-07-10
HUCDu10.output	Output file for HU/RT/CD SIFs (load step 10)	05-04-10	05-07-10
HUCDu11.output	Output file for HU/RT/CD SIFs (load step 11)	05-04-10	05-07-10
HUCDu12.output	Output file for HU/RT/CD SIFs (load step 12)	05-04-10	05-07-10
HUCDu13.output	Output file for HU/RT/CD SIFs (load step 13)	05-04-10	05-07-10
HUCDu14.output	Output file for HU/RT/CD SIFs (load step 14)	05-04-10	05-07-10
HUCDu15.output	Output file for HU/RT/CD SIFs (load step 15)	05-04-10	05-07-10
HUCDu16.output	Output file for HU/RT/CD SIFs (load step 16)	05-04-10	05-07-10
HUCDu17.output	Output file for HU/RT/CD SIFs (load step 17)	05-04-10	05-07-10

File Name	Description	Modified Date	Installed Date
HUCDu18.output	Output file for HU/RT/CD SIFs (load step 18)	05-04-10	05-07-10
RWAu1.output	Output file for RWA SIFs (load step 1)	04-05-10	05-07-10
RWAu2.output	Output file for RWA SIFs (load step 2)	04-05-10	05-07-10
RWAu3.output	Output file for RWA SIFs (load step 3)	04-05-10	05-07-10
RWAu4.output	Output file for RWA SIFs (load step 4)	04-05-10	05-07-10

ANSYS Verification

File Name	Description	Modified Date	Installed Date
vm161.vrt	Verification problem for thermal analysis	04-07-10	05-07-10
vm148.vrt	Verification problem for stress analysis	04-07-10	05-07-10
vm143.vrt	Verification problem for stress intensity factor	04-07-10	05-07-10

APPENDIX C: FINITE ELEMENT CRACK MODEL

C.1 Introduction

A non-radial partial penetration nozzle in a spherically shaped pressure vessel presents a challenging set of geometric constraints for both stress analysis and fracture mechanics analysis of flaws, especially in the J-groove weld. Since there are no closed-form solutions available to calculate stress intensity factors for such flaws, a three-dimensional finite element crack model is developed in this appendix for use in evaluating "J-shaped" flaws in the area of the partial penetration attachment weld.

The three-dimensional finite element model is constructed using crack tip elements along the entire J-shaped crack front, extending from the inside surface of the cladding to the bored surface of the penetration. An uncracked model of the nozzle, J-groove weld and butter, and a portion of the reactor vessel head and cladding is first created using the ANSYS finite element computer program [6]. After removing a block of elements around the crack front and inserting a sub-model of crack tip elements, stress intensity factors can be obtained via the program's KCALC routine. The crack tip sub-model consists of 20-node isoparametric elements that are collapsed to form wedges, with the appropriate mid-side nodes shifted to quarter-point locations to create a $1/\sqrt{r}$ singularity in strain at the crack tip.

C.2 Base Finite Element Model

A three-dimensional finite element model is constructed to represent an uncracked non-radial nozzle penetration in a hemi-spherical shaped head. This model utilizes the ANSYS SOLID95 3-D 20-node structural solid element, exclusively, so that a portion of the model can be readily removed and replaced with a crack tip sub-model.

C.2.1 Geometry

As shown in Figure C-1, the model is a 180-degree segment of the head, cladding, weld butter, and J-groove weld.

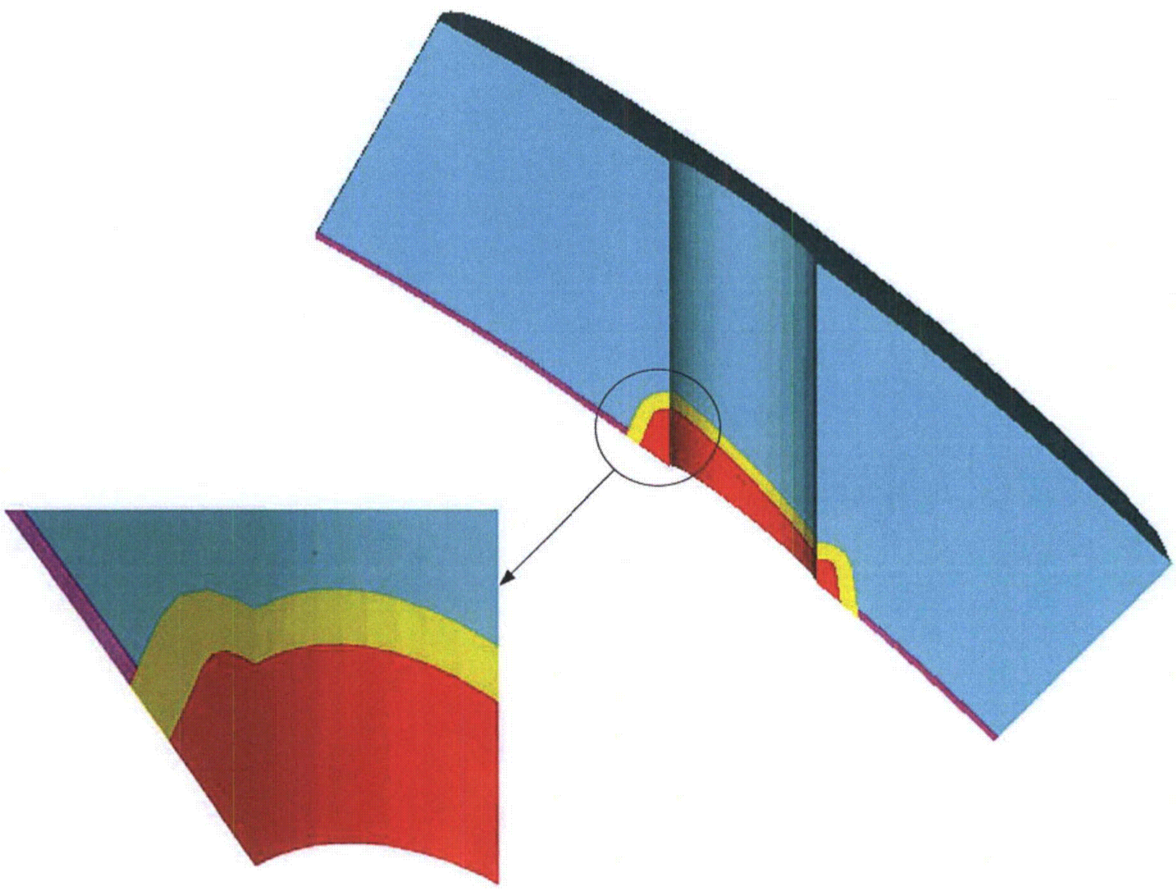

Figure C-1: Overall Model of Reactor Vessel Head Penetration

Key dimensions are:

Radius to base metal = { } in. [14]
Head thickness (minimum) = { } in. [14]
Cladding thickness (nominal) = { } in. [15]
Butter thickness (nominal) = { } in. [16] or { }
Hole diameter (original) = { } in. [16] (near { } after machining [1])
J-groove weld center diameter = { } in. [16]
J-groove weld angle = { } deg. [16]
Basic J-groove radius = { } in. [16]
Basic J-groove height = { } in. [16] { }"
Additional height to base metal (nom.) = { } in. [16] or { }
Horizontal distance to outermost nozzle = { } in. [16]
Penetration angle at outermost nozzle = { } deg.

C.2.2 Materials

The material designations of the various components of the model are:

Component	Material
RV head	SA-533 Grade B Class 1 [2]
Cladding	Stainless steel (use Type 316 properties)
J-groove weld filler	Alloy 182 [2] (use Alloy 600 properties for SB-167)
J-groove weld butter	Alloy 182 [2] (use Alloy 600 properties for SB-167)

The mechanical and thermal properties for these materials are provided in Section 4.1.1.

C.2.3 Boundary Conditions

The model includes a 180-degree segment of the weld and adjacent portions of the head. The vertical plane containing the vertical axes of the reactor vessel and the outermost penetration forms a plane of symmetry for the model. The displacements normal to this plane of symmetry are fixed (in the global Z-direction). Displacement constraints are also applied to the outer peripheral boundary of the spherical segment to simulate a state of membrane stress. By specifying meridional displacements to be zero in a spherical coordinate system, the head can only displace along a spherical radius parallel to this boundary.

C.3 Finite Element Crack Models

The three-dimensional finite element crack model is developed by removing a portion of the head and butter and inserting a sub-model of crack tip elements, as illustrated in Figure C-2. Displacement constraints are also removed along the plane of symmetry for nodes on the crack face. Figure C-3 shows the final crack model used to analyze a postulated flaw in the J-groove weld and butter.

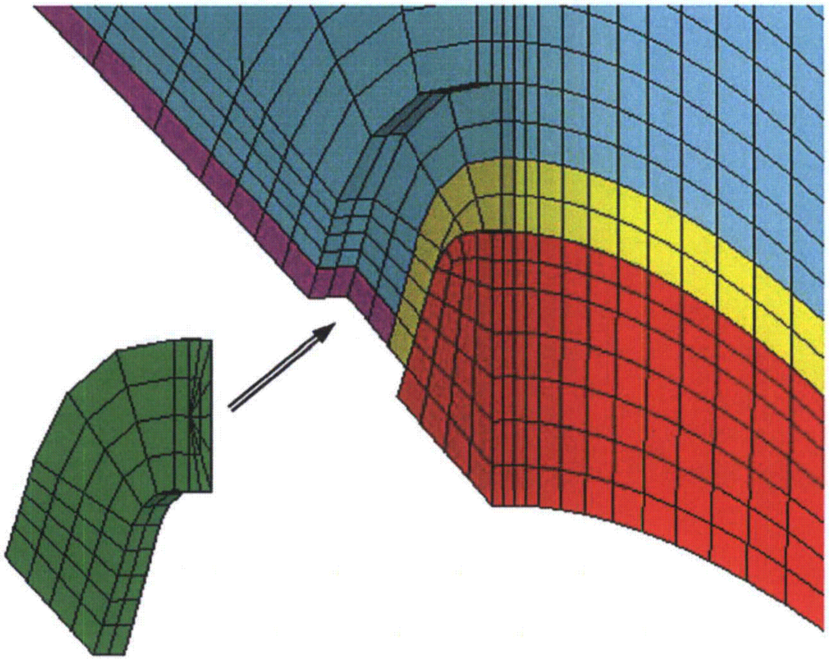

Figure C-2: Development of Crack Model

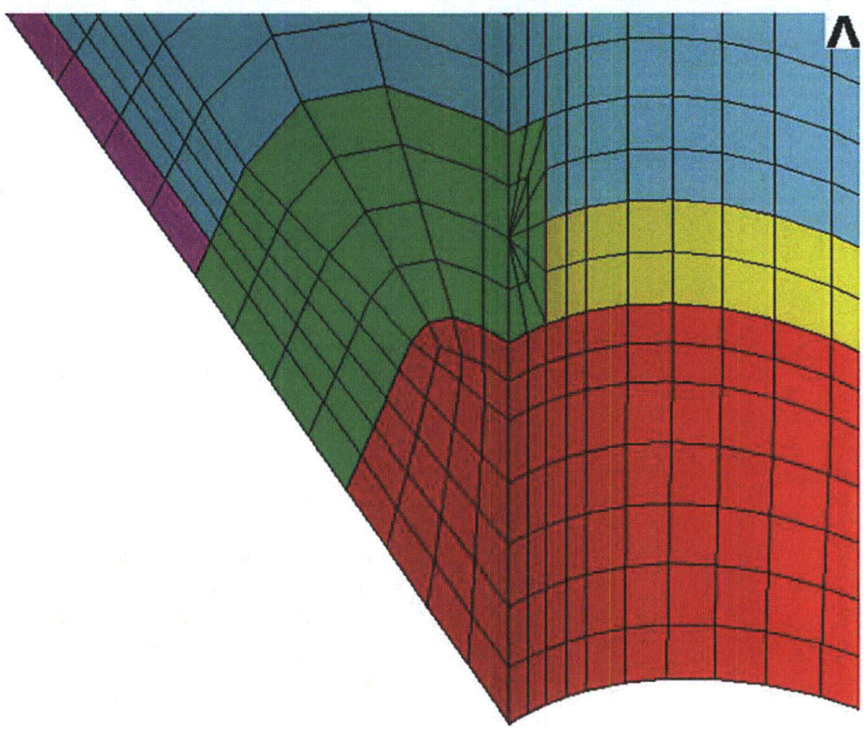

Figure C-3: Final Finite Element Crack Model

APPENDIX D: FINITE ELEMENT STRESS MODEL

A three-dimensional linear-elastic finite element model is developed for use in obtaining operational stresses from transient loading conditions. The origin of this model is the uncracked stress model described in Section C.2, prior to transformation to a crack model. The ANSYS SOLID95 3-D 20-node structural solid elements of the stress model are converted to SOLID90 3-D 20-node thermal solid elements to create a thermal model for use in transient analysis to calculate nodal temperatures.

Three heat transfer regions are defined for applying thermal loads to the model in the form of time-dependent bulk fluid temperatures and convective heat transfer coefficients (HTC). Figure D-1 identifies these regions at the inside surface of the cladding, the bored surface of the head at the location of the nozzle, and the outside surface of the head. Table D-1 lists the bulk fluid temperatures and heat transfer coefficients for the heatup/reactor trip/cooldown full-range transient used in the present flaw evaluations. Table D-2 provides similar data for the rod withdrawal accident transient. Temperature-time history plots are presented in Figure D-2 and Figure D-3 for both transients.

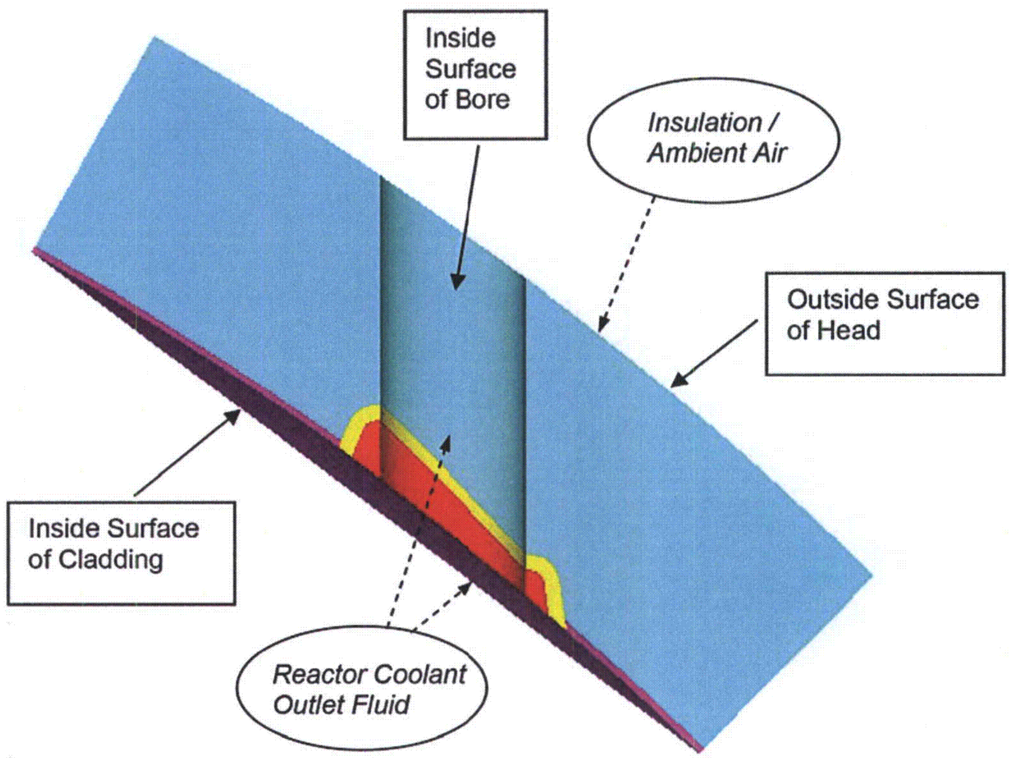

Figure D-1: Heat Transfer Regions of Thermal Model

Table D-1: Heatup/Reactor Trip/Cooldown Transient Definition

References: Section III Stress Analysis [20] and RCS Functional Specification [17]

Load Step	Time (hr.)	Inside Temp. (°F)	Outside Temp. (°F)	Inside Cladding HTC (Btu/hr/in^2-°F)	Inside Bore HTC (Btu/hr/in^2-°F)	Outside Head HTC (Btu/hr/in^2-°F)	Comment
1							
2							
3							heatup
4							
5							
6							SS at 8% power
7							power increase
8							SS at 100% power
9							
10							
11							
12							reactor trip
13							
14							
15							
16							
17							cooldown
18							
19							

Table D-2: Rod Withdrawal Accident Transient Definition

References: Section III Stress Analysis [20] and RCS Functional Specification [17]

Load Step	Time (hr.)	Inside Temp. (°F)	Outside Temp. (°F)	Inside Cladding HTC (Btu/hr/in^2-°F)	Inside Bore HTC (Btu/hr/in^2-°F)	Outside Head HTC (Btu/hr/in^2-°F)	Comment
1							
2							
3							
4							
5							
6							
7							
8							
9							

Figure D-2: Heatup/Reactor Trip/Cooldown Temperature-Time History

Figure D-3: Rod Withdrawal Accident Temperature-Time History

APPENDIX E: STRESS INTENSITY FACTOR DUE TO PRESSURE

The elastic-plastic fracture flaw evaluations of Section 5.3 utilize different safety factors for primary (pressure) and secondary stress (residual and thermal) intensity factors. In order to isolate the pressure term, K_{Ip}, stress intensity factors are developed for an arbitrary pressure load of 2500 psig at 600 °F.

Table E-1 presents stress intensity factors at the ten crack front positions defined in Figure 2-2. Since these values were determined for the initial crack size, they are adjusted by the square root of the crack size, considering the final crack size after four years of crack growth, in the same fashion as described in Section 2.1.3.

The K_{Ip} pressure terms used in the EPFM flaw evaluations of Section 5.3 are derived below.

Let, $$K_{Ip}(a,P) = K_{Ip}(a_o,P_o)\sqrt{\frac{a}{a_o}} \times \frac{P}{P_o}$$

Temperature,	$T = 600\ ^\circ F$
Pressure,	$P_o = 2500$ psig
Initial flaw size,	$a_o = 2.035$ in.
From Table E-1,	$K_{Ip}(a_o,P_o) = 56.952\ ksi\sqrt{in}$

Controlling Transients	Shutdown	Heatup/Cooldown w/ Reactor Trip (RT2)	Rod Withdrawal Accident
Temperature,	$T = 70\ ^\circ F$	{ } °F	{ } °F
Pressure,	$P = 0$ psig	{ } psig	{ } psig
Final flaw size,	$a = 2.1108$ in.	2.1108 in.	2.1108 in.
Final stress intensity factor,	$K_{Ip}(a,P) = 0\ ksi\sqrt{in}$	$39.906\ ksi\sqrt{in}$	$63.687\ ksi\sqrt{in}$

Table E-1: Stress Intensity Factors for Internal Pressure Loading

Temperature =	600	F
Pressure =	2500	psig
Flaw size =	2.035	in.

	Position	SIF (ksi√in)
Inside Surface	1	56.697
	2	51.258
	3	49.563
	4	48.028
	5	46.116
	6	43.286
	7	39.883
	8	41.978
	9	50.267
Bored Surface	10	56.952